

1 **Title page**

2 Title:

3 Stretch Regulates Alveologenesis and Homeostasis Via Mesenchymal G_{αq/11}-Mediated
4 TGFβ2 Activation

5 **Authors:**

6 Amanda T Goodwin^{1*}

7 Alison E John²

8 Chitra Joseph¹

9 Anthony Habgood¹

10 Amanda L Tatler¹

11 Katalin Susztak³

12 Matthew Palmer⁴

13 Stefan Offermanns⁵

14 Neil C Henderson^{6,7}

15 R Gisli Jenkins²

16 1) School of Medicine, University of Nottingham, UK

17 2) National Heart and Lung Institute, Imperial College London, UK

18 3) Department of Medicine, Division of Nephrology, University of Pennsylvania
19 Perelman School of Medicine, Philadelphia, USA

20 4) Department of Pathology, Division of Nephrology, University of Pennsylvania
21 Perelman School of Medicine, Philadelphia, USA

22 5) Max Planck Institute for Heart and Lung Research, Bad Nauheim, Germany

23 6) Centre for Inflammation Research, University of Edinburgh, UK

24 7) MRC Human Genetics Unit, Institute of Genetics and Molecular Medicine, University
25 of Edinburgh, Edinburgh, UK.

26 ***Correspondence to:** Amanda T Goodwin – Amanda.Goodwin@nottingham.ac.uk

27

28 **Key words:** Alveologenesis; TGFβ; G_{αq/11}; GPCR; lung development; cyclical mechanical
29 stretch

30 **Word count:** 6617

31 **Summary statement**

32 Mesenchymal cell $G_{\alpha q/11}$ signalling regulates myofibroblast function and stretch-mediated
33 TGF β 2 signalling, which are important for alveologenesis and organ homeostasis. These
34 mechanisms are relevant to both developmental and adult lung disease.

35 **Abstract**

36 Alveolar development and repair require tight spatiotemporal regulation of numerous
37 signalling pathways that are influenced by chemical and mechanical stimuli. Mesenchymal
38 cells play key roles in numerous developmental processes. Transforming growth factor- β
39 (TGF β) is essential for alveologenesis and lung repair, and the G protein α subunits $G_{\alpha q}$ and
40 $G_{\alpha 11}$ ($G_{\alpha q/11}$) transmit mechanical and chemical signals to activate TGF β in epithelial cells. To
41 understand the role of mesenchymal $G_{\alpha q/11}$ in lung development, we generated constitutive
42 (*Pdgfrb-Cre^{+/-};Gnaq^{fl/fl};Gna11^{-/-}*) and inducible (*Pdgfrb-Cre/ERT2^{+/-};Gnaq^{fl/fl};Gna11^{-/-}*)
43 mesenchymal $G_{\alpha q/11}$ deleted mice. Mice with constitutive $G_{\alpha q/11}$ gene deletion exhibited
44 abnormal alveolar development, with suppressed myofibroblast differentiation, altered
45 mesenchymal cell synthetic function, and reduced lung TGF β 2 deposition, as well as kidney
46 abnormalities. Tamoxifen-induced mesenchymal $G_{\alpha q/11}$ gene deletion in adult mice resulted
47 in emphysema associated with reduced TGF β 2 and elastin deposition. Cyclical mechanical
48 stretch-induced TGF β activation required $G_{\alpha q/11}$ signalling and serine protease activity, but
49 was independent of integrins, suggesting an isoform-specific role for TGF β 2. These data
50 highlight a previously undescribed mechanism of cyclical stretch-induced $G_{\alpha q/11}$ -dependent
51 TGF β 2 signalling in mesenchymal cells, which is imperative for normal alveologenesis and
52 maintenance of lung homeostasis.

53 **Introduction**

54 Normal alveologenesis requires tight spatiotemporal control of numerous molecular
55 signalling pathways, and coordinated crosstalk between multiple cell types. Any perturbation
56 to these complex processes can disrupt alveolar formation, resulting in structural and
57 functional abnormalities to the gas exchange regions of the lungs. Such abnormalities
58 contribute to perinatal death and lifelong lung function disturbances in survivors (Lovering et
59 al. 2014). The alveolar stage is the final phase of lung development, during which primitive
60 pulmonary sacculi are divided by newly formed secondary septae to form mature alveoli.
61 Alveolarisation occurs between 36 weeks gestation to around 6 years of age in humans

62 (Donahoe, Longoni, and High 2016), and postnatal days 3-30 (P3-P30) in mice (Beauchemin
63 et al. 2016; Pozarska et al. 2017; C. Li et al. 2015), therefore postnatal exposures and
64 stimuli are key influences in alveolar development. Many pathways that drive normal lung
65 development are also instrumental in adult lung repair (Chanda et al. 2019), therefore
66 understanding normal lung development could have implications for numerous pulmonary
67 diseases.

68 Pericytes are perivascular cells that are widely considered to be mesenchymal precursor
69 cells in the lung, and are integral to multiple developmental processes (Kato et al. 2018;
70 Barron, Gharib, and Duffield 2016; Ricard et al. 2014). Pericytes express platelet-derived
71 growth factor- β (PDGFR β), PDGFR α , and NG2, among other markers, but the most specific
72 marker for pericytes is PDGFR β (Ricetti et al. 2020). Pericytes migrate and differentiate into
73 parenchymal myofibroblasts in the lung, and myofibroblast-driven deposition of extracellular
74 matrix (ECM) proteins, such as collagen and elastin, provide the essential scaffolds for
75 secondary septation during lung development and lung repair (Mecham 2018; Mizikova and
76 Morty 2015). Therefore pericytes, and the mesenchymal cells that derive from them, are
77 instrumental in alveologenesi s and lung homeostasis.

78 The pleiotropic cytokine transforming growth factor- β (TGF β) regulates numerous
79 developmental and repair processes, including the proliferation, migration, and differentiation
80 of pericytes (Bartram and Speer 2004), and the generation of ECM. TGF β signalling is tightly
81 regulated in vivo by the production of TGF β in latent form, and the three mammalian TGF β
82 isoforms must be activated to exert their biological effects. While TGF β signalling is essential
83 for multiple processes in alveolar development and repair (Bartram and Speer 2004), the
84 mechanisms that control TGF β activation in alveologenesi s are unclear.

85 Latent TGF β is activated when a conformational change to the large latent complex alters
86 the relationship between TGF β and the latency associated peptide, allowing TGF β to
87 interact with its receptor. The G-proteins G $_{\alpha q}$ and G $_{\alpha 11}$ (G $_{\alpha q/11}$) mediate TGF β activation in
88 response to G-protein-coupled receptor (GPCR)-ligand binding as well as mechanical
89 stretch in epithelial cells (Xu et al. 2009; John et al. 2016). GPCR signalling has also been
90 implicated in normal alveologenesi s (Funke et al. 2016). Cyclical mechanical stretch (CMS)
91 has been shown to induce TGF β activation in lung slices via a Rho-associated kinase
92 (ROCK) - and αv integrin-dependent process (Froese et al. 2016), although the contribution
93 to this by individual cell types is unknown. While stretch secondary to foetal breathing
94 movements in utero is essential for early lung development (Donahoe, Longoni, and High
95 2016), the role of breathing-related CMS specifically in mesenchymal cells in alveolar
96 development and the maintenance of adult alveoli has not been investigated.

97 We hypothesised that $G_{\alpha q/11}$ would mediate CMS-induced TGF β activation via ROCK and
98 integrin signalling in mesenchymal cells, and that this would be important in alveologenesi
99 Here we show, using mesenchymal $G_{\alpha q/11}$ knockout mouse models and an in vitro CMS
100 system, that mesenchymal $G_{\alpha q/11}$ is essential for normal alveologenesi and maintenance of
101 adult alveoli via CMS-induced TGF β signalling, but that this occurs in a ROCK- and integrin-
102 independent manner via a pathway likely to involve the TGF β 2 isoform.

103 **Results**

104 ***Pdgfrb-Cre^{+/-};Gnaq^{fl/fl};Gna11^{-/-}* mice are growth restricted and are not viable beyond** 105 **P24**

106 To understand whether mesenchymal $G_{\alpha q/11}$ deletion resulted in detrimental effects in vivo,
107 gross phenotypes and genotype frequencies of offspring from the *Pdgfrb-Cre^{+/-}* x
108 *Gnaq^{fl/fl};Gna11^{-/-}* crosses were analysed. Fewer mesenchymal $G_{\alpha q/11}$ knockout (*Pdgfrb-Cre^{+/-}*
109 *;Gnaq^{fl/fl};Gna11^{-/-}*) pups reached genotyping age (P14) than was expected (6.6% observed
110 compared with 12.5% expected, Chi squared value = 22.03, $p < 0.005$, **Figure 1A**).

111 Conversely, mice with at least one functional mesenchymal *Gnaq* or *Gna11* allele reached
112 genotyping age at rates closer to the expected Mendelian frequencies (**Figure 1A**).

113 Furthermore, *Pdgfrb-Cre^{+/-};Gnaq^{fl/fl};Gna11^{-/-}* pups were notably smaller than littermates with
114 at least one intact mesenchymal *Gnaq* or *Gna11* allele. *Pdgfrb-Cre^{+/-};Gnaq^{fl/fl};Gna11^{-/-}*
115 animals had a mean weight 1.9-3.2g lower than all other genotypes (5.4g vs 7.3-8.4g,
116 $p < 0.03$ **Figure 1B**). *Pdgfrb-Cre^{+/-};Gnaq^{fl/fl};Gna11^{-/-}* pups were also smaller in physical size
117 compared with control animals (**Figure 1C**). There was no sex-related difference in weight
118 across genotypes (**Figure 1D**). These findings indicate that mesenchymal $G_{\alpha q/11}$ deletion
119 causes a detrimental developmental phenotype, leading to death in utero or in early life.

120 The first two *Pdgfrb-Cre^{+/-};Gnaq^{fl/fl};Gna11^{-/-}* mice from this breeding programme were
121 humanely killed due to poor physical condition at P21 and P24. Therefore, all further
122 analyses were performed in P14 mice, before evidence of ill health was observed.
123 *Gnaq^{fl/fl};Gna11^{-/-}* mice develop normally and do not express a phenotype (John et al. 2016),
124 therefore *Gnaq^{fl/fl};Gna11^{-/-}* littermates were used as controls for all analyses (from here
125 referred to as *Gna11^{-/-}* controls).

126 ***Pdgfrb-Cre^{+/-};Gnaq^{fl/fl};Gna11^{-/-}* mice have impaired alveologenesi.**

127 To understand the role of mesenchymal $G_{\alpha q/11}$ signalling in lung development, the lungs of
128 *Pdgfrb-Cre^{+/-};Gnaq^{fl/fl};Gna11^{-/-}* mice and *Gna11^{-/-}* controls were examined histologically.
129 *Pdgfrb-Cre^{+/-};Gnaq^{fl/fl};Gna11^{-/-}* mouse lungs exhibited clear abnormalities consistent with

130 impaired alveolar development at P14 (**Figure 2A**). *Pdgfrb-Cre^{+/-};Gnaq^{fl/fl};Gna11^{-/-}* lungs
131 contained enlarged airspaces with a mean linear intercept distance of 63.47 μ m compared
132 with 36.43 μ m in *Gna11^{-/-}* mice (p=0.03, **Figure 2B**), thickened alveolar walls of 12.2 μ m
133 compared with 7.0 μ m in *Gna11^{-/-}* controls (p=0.03, **Figure 2C**), and fewer secondary crests
134 (53.7 vs 107.2 per field, p=0.03, **Figure 2D**) relative to *Gna11^{-/-}* littermate controls.

135 In addition to these structural abnormalities, *Pdgfrb-Cre^{+/-};Gnaq^{fl/fl};Gna11^{-/-}* lungs expressed
136 lower levels of the proliferative marker Ki67 than *Gna11^{-/-}* controls, with 16% of cell nuclei
137 staining positively for Ki67 in *Pdgfrb-Cre^{+/-};Gnaq^{fl/fl};Gna11^{-/-}* lungs compared with 26% in
138 *Gna11^{-/-}* controls (p=0.03, **Figure 2A, 2E**). Furthermore, *Pdgfrb-Cre^{+/-};Gnaq^{fl/fl};Gna11^{-/-}* lungs
139 contained a lower proportion of cells staining positively for the type II epithelial cell marker
140 pro-surfactant protein C (pro-SPC) than *Gna11^{-/-}* control lungs, at 8.9% and 12.8% of all
141 cells, respectively (**Figure 2A, 2F**).

142 Finally, *Pdgfrb-Cre^{+/-};Gnaq^{fl/fl};Gna11^{-/-}* lungs were heavier relative to total body weight
143 compared with lungs from *Gna11^{-/-}* mice (16.5 vs 14.3mg/g total body weight, p<0.01,
144 **Figure 2G**), suggesting elevated lung density in these animals. Overall, these structural,
145 proliferative, and cellular differentiation abnormalities indicate a disturbance to
146 alveologenesis in *Pdgfrb-Cre^{+/-};Gnaq^{fl/fl};Gna11^{-/-}* mice.

147 **Myofibroblast differentiation and function is defective in *Pdgfrb-Cre^{+/-};Gnaq^{fl/fl};Gna11^{-/-}*** 148 **mouse lungs**

149 Myofibroblasts are essential for normal alveolar development, therefore studies were
150 undertaken to assess myofibroblast differentiation and function in *Pdgfrb-Cre^{+/-}*
151 *;Gnaq^{fl/fl};Gna11^{-/-}* lungs.

152 Immunohistochemical staining for the myofibroblast marker α -smooth muscle actin (α SMA)
153 demonstrated fewer myofibroblasts in the lungs of P14 *Pdgfrb-Cre^{+/-};Gnaq^{fl/fl};Gna11^{-/-}* mice
154 compared with *Gna11^{-/-}* littermate controls (**Figure 3A**). While overall α SMA staining was
155 decreased in *Pdgfrb-Cre^{+/-};Gnaq^{fl/fl};Gna11^{-/-}* lungs, there was no significant reduction in the
156 proportion of α SMA-positive secondary crests compared with *Gna11^{-/-}* lungs (0.69 vs 0.84 in
157 controls, p =0.2, **Figure 3B**).

158 To investigate whether $G_{\alpha q/11}$ knockout influences myofibroblast differentiation, murine
159 embryonic fibroblasts (MEFs) that were wild-type (WT), $G_{\alpha q/11}$ deficient (*Gnaq^{-/-};Gna11^{-/-}*) or
160 $G_{\alpha 12/13}$ deficient (*Gna12^{-/-};Gna13^{-/-}*) were assessed for α SMA protein and Acta2 mRNA
161 expression. MEFs with a long-term deficiency in $G_{\alpha q/11}$ had lower Acta2 mRNA (**Figure 3C**)
162 and α SMA protein expression than WT MEFs, whereas MEFs lacking $G_{\alpha 12/13}$, another G_{α}
163 subunit family, did not have significantly different α SMA expression compared with WT cells

164 (Figure 3D, 3E). This implies a key role for $G_{\alpha q/11}$ signalling in the differentiation of
165 myofibroblasts from mesenchymal precursor cells.

166 *Pdgfrb-Cre^{+/-};Gnaq^{fl/fl};Gna11^{-/-}* lungs also showed evidence of defective myofibroblast
167 synthetic function. *Pdgfrb-Cre^{+/-};Gnaq^{fl/fl};Gna11^{-/-}* lungs contained fewer elastin fibres (7.4 vs
168 24.9 fibres per field, $p=0.03$, Figure 3A & 3F) and fewer elastin-positive secondary crests
169 (57.5% vs 84.8%, $p=0.03$, Figure 3G) than *Gna11^{-/-}* mouse lungs. Furthermore, picrosirius
170 red staining revealed that P14 *Pdgfrb-Cre^{+/-};Gnaq^{fl/fl};Gna11^{-/-}* mouse lungs contained less
171 collagen than the lungs of *Gna11^{-/-}* controls (Figure 3A). These data were supported by
172 lower *Eln*, *Col1a1* and *Col3a1* mRNA expression in *Gnaq^{-/-};Gna11^{-/-}* MEFs than WT MEFs
173 (Figure 3H-J). These findings imply a failure of myofibroblast differentiation in the lungs of
174 mice lacking mesenchymal $G_{\alpha q/11}$ associated with a reduction in myofibroblast function,
175 leading to a reduction in subepithelial matrix deposition.

176 ***Pdgfrb-Cre^{+/-};Gnaq^{fl/fl};Gna11^{-/-}* mice have abnormal peripheral pulmonary vessels**

177 Pericytes are important precursor cells to pulmonary myofibroblasts, and originate in the
178 perivascular region. Therefore, we examined the pulmonary vasculature histologically to
179 assess for abnormalities caused by mesenchymal $G_{\alpha q/11}$ deletion. P14 *Pdgfrb-Cre^{+/-}*
180 *;Gnaq^{fl/fl};Gna11^{-/-}* lungs contained markedly abnormal peripheral pulmonary vessels (Figure
181 4A-G), with significantly thicker walls than the peripheral pulmonary vessels of *Gna11^{-/-}*
182 controls (mean maximum wall thickness 16.4 vs 7.3 μ m, $p=0.03$, Figure 4H). These vessels
183 consisted of a thin CD31 positive endothelial layer (Figure 4B) surrounded by a thickened
184 α SMA positive vascular smooth muscle layer (Figure 4C) without increased proliferation
185 (Ki67 positive; Figure 4D), indicating that the smooth muscle layer was hypertrophic rather
186 than hyperplastic. These abnormal vessels did not contain significant collagen or elastin
187 layers (Figure 4E-G). In contrast, the alveolar capillaries of *Pdgfrb-Cre^{+/-};Gnaq^{fl/fl};Gna11^{-/-}*
188 lungs had a similar appearance to those seen in *Gna11^{-/-}* lungs (Figure 4J).

189 Given the similarity in appearance of the abnormal peripheral pulmonary vasculature in
190 *Pdgfrb-Cre^{+/-};Gnaq^{fl/fl};Gna11^{-/-}* lungs to those seen in pulmonary arterial hypertension, we
191 assessed the hearts from these animals for evidence of right ventricular hypertrophy. We
192 found no difference in right: left ventricular wall ratio in *Pdgfrb-Cre^{+/-};Gnaq^{fl/fl};Gna11^{-/-}* mice
193 relative to controls (Figure 4K-L). These data suggest a primary *Pdgfrb⁺* cell-driven defect,
194 rather than secondary pulmonary hypertension due to impaired alveologenesis.

195 ***Pdgfrb-Cre^{+/-};Gnaq^{fl/fl};Gna11^{-/-}* mice have kidney abnormalities**

196 As *Pdgfrb* expression is not exclusive to lung mesenchymal cells, the kidneys, hearts, livers,
197 and bowel of *Pdgfrb-Cre^{+/-};Gnaq^{fl/fl};Gna11^{-/-}* mice were assessed for extrapulmonary
198 abnormalities.

199 We observed an expansion and prominence of medullary mesenchymal cells in *Pdgfrb-Cre^{+/-}*
200 *;Gnaq^{fl/fl};Gna11^{-/-}* kidneys demonstrated by α SMA and PDGFR β staining (**Figure 5A**), with
201 associated thinning of the cortex (median cortex: medulla ratio 0.31 in *Pdgfrb-Cre^{+/-}*
202 *;Gnaq^{fl/fl};Gna11^{-/-}* kidneys and 0.43 in *Gna11^{-/-}* controls, $p < 0.03$, **Figure 5B, C**). The relative
203 kidney to total body weight values of *Pdgfrb-Cre^{+/-};Gnaq^{fl/fl};Gna11^{-/-}* mouse kidneys were not
204 different to *Gna11^{-/-}* controls (median kidney: total body weight ratio 7.3 in *Pdgfrb-Cre^{+/-}*
205 *;Gnaq^{fl/fl};Gna11^{-/-}* mice and 6.5 in *Gna11^{-/-}* controls, $p = 0.55$; **Figure 5D**). These data suggest
206 that mesenchymal $G_{\alpha q/11}$ is important in normal kidney development.

207 *Pdgfrb-Cre^{+/-};Gnaq^{fl/fl};Gna11^{-/-}* mice had normal heart, liver and bowel histology (Figure S1),
208 suggesting that mesenchymal $G_{\alpha q/11}$ signalling is not required for normal heart, liver, or bowel
209 development or homeostasis from conception to P14 in mice.

210 **Mice with mesenchymal $G_{\alpha q/11}$ knockout induced in adulthood have emphysema with**
211 **altered ECM, but no extrapulmonary abnormalities**

212 To assess whether the abnormalities seen in *Pdgfrb-Cre^{+/-};Gnaq^{fl/fl};Gna11^{-/-}* mice were
213 related solely to disturbed organ developmental processes or could also affect mature lungs,
214 a tamoxifen-inducible mesenchymal $G_{\alpha q/11}$ knockout model (*Pdgfrb-Cre/ERT2^{+/-}*
215 *;Gnaq^{fl/fl};Gna11^{-/-}*) was conducted in adult mice (**Figure 6A**).

216 Tamoxifen-naïve *Pdgfrb-Cre/ERT2^{+/-};Gnaq^{fl/fl};Gna11^{-/-}* mice were born at the expected
217 frequency. According to the supplier, it is expected that 20% of offspring from breeding of the
218 Cre-expressing hemizygous mice with wild type mice will express the *Pdgfrb-Cre/ERT2*
219 transgene (Laboratory), rather than the 50% Cre-expression rate observed in the germline
220 *Pdgfrb-Cre^{+/-}* mouse colony. The frequency of *Pdgfrb-Cre/ERT2^{+/-};Gnaq^{fl/fl};Gna11^{-/-}* mice
221 reaching genotyping age was 6.4%, compared with the expected 5% (total number of mice
222 born 109; **Figure 6B**). This indicates that having the *Pdgfrb-Cre/ERT2^{+/-};Gnaq^{fl/fl};Gna11^{-/-}*
223 genotype, without administration of tamoxifen, does not cause any gross developmental
224 defects.

225 When a three week course of tamoxifen was administered to P49 *Pdgfrb-Cre/ERT2^{+/-}*
226 *;Gnaq^{fl/fl};Gna11^{-/-}* mice (n=4, 1 female 3 male), no detrimental effect to health status was
227 observed compared with littermate controls. Furthermore, *Pdgfrb-Cre/ERT2^{+/-}*
228 *;Gnaq^{fl/fl};Gna11^{-/-}* mice gained weight at the same rate as littermate controls with the other
229 genotypes during the tamoxifen protocol (median weight on day 21 of tamoxifen 104.3% of

230 baseline in *Pdgfrb-Cre/ERT2^{+/-};Gnaq^{fl/fl};Gna11^{-/-}* mice compared to 106.2% of baseline in
231 other genotypes, $p=0.71$; **Figure 6C**). A small reduction in weight was observed early in the
232 tamoxifen protocol that was independent of genotype and was in keeping with a change in
233 diet (Kiermayer et al. 2007). These data suggest that short-term mesenchymal $G_{\alpha q/11}$
234 knockout does not cause gross physiological disturbances *in vivo*.

235 On histological analysis, the lungs of *Pdgfrb-Cre/ERT2^{+/-};Gnaq^{fl/fl};Gna11^{-/-}* mice treated with
236 tamoxifen demonstrated increased airspace size compared with *Gna11^{-/-}* controls (mean
237 linear intercept distance $52.5\mu\text{m}$ in *Pdgfrb-Cre/ERT2^{+/-};Gnaq^{fl/fl};Gna11^{-/-}* mice compared with
238 $39.3\mu\text{m}$ in *Gna11^{-/-}* controls, $p=0.03$, **Figure 6D, 6E**), suggestive of emphysema. *Pdgfrb-*
239 *Cre/ERT2^{+/-};Gnaq^{fl/fl};Gna11^{-/-}* lungs contained fewer elastin fibres than *Gna11^{-/-}* controls after
240 three weeks of tamoxifen (median number of elastin fibres per high powered field 13.0 in
241 *Pdgfrb-Cre/ERT2^{+/-};Gnaq^{fl/fl};Gna11^{-/-}* mice compared with 26.9 in *Gna11^{-/-}* controls, $p=0.03$,
242 **Figure 6D, 6F**), similar to the constitutive knockout. In contrast, *Pdgfrb-Cre/ERT2^{+/-}*
243 *;Gnaq^{fl/fl};Gna11^{-/-}* lungs did not exhibit altered collagen deposition or evidence of fewer
244 myofibroblasts (αSMA) when compared with *Gna11^{-/-}* controls (**Figure 6D**). Three of the four
245 *Pdgfrb-Cre/ERT2^{+/-};Gnaq^{fl/fl};Gna11^{-/-}* mice also exhibited abnormal pulmonary mononuclear
246 cellular aggregates which predominated at the pleural surfaces (**Figure 6G**), and were not
247 observed in littermate control mice. Despite these abnormalities, *Pdgfrb-Cre/ERT2^{+/-}*
248 *;Gnaq^{fl/fl};Gna11^{-/-}* mice did not exhibit signs of respiratory distress.

249 In contrast with *Pdgfrb-Cre^{+/-};Gnaq^{fl/fl};Gna11^{-/-}* mice, *Pdgfrb-Cre/ERT2^{+/-};Gnaq^{fl/fl};Gna11^{-/-}*
250 mice administered tamoxifen did not exhibit any renal abnormalities on histology (**Figure**
251 **S2**). This implies that mesenchymal $G_{\alpha q/11}$ is needed for normal kidney development, but not
252 maintenance of the normal kidney.

253 **Cyclical mechanical stretch-induced TGF β activation in fibroblasts requires $G_{\alpha q/11}$, but** 254 **not ROCK or αv or $\beta 1$ integrins**

255 Given the crucial roles TGF β in alveolar development, lung repair, and pericyte migration
256 and differentiation, we investigated the role of mesenchymal $G_{\alpha q/11}$ in a cyclical stretch model
257 of TGF β activation. Mesenchymal cells with and without intact $G_{\alpha q/11}$ signalling were
258 subjected to breathing-related CMS and TGF β signalling was assessed. CMS-induced TGF β
259 signalling, as assessed by Smad2 phosphorylation, was significantly reduced in *Gnaq^{-/-}*
260 *;Gna11^{-/-}* MEFs compared with WT MEFs (**Figure 7A-B**). This finding was specific to the
261 $G_{\alpha q/11}$ family of G proteins, as there was no effect of $G_{\alpha 12/13}$ knockdown on stretch-induced
262 TGF β signalling in MEFs (**Figure 7A**).

263 To validate the role of $G_{\alpha q/11}$ in stretch-induced TGF β signalling in mesenchymal cells across
264 species, human lung fibroblasts (HLFs) with and without siRNA-induced *GNAQ* and *GNA11*

265 knockdown were subjected to breathing-related CMS. *GNAQ* and *GNA11* siRNA led to
266 substantial reductions in both $G_{\alpha q}$ and $G_{\alpha 11}$ protein expression in HLFs, and significantly
267 reduced CMS-induced TGF β signalling compared with scrambled control (Scr) siRNA as
268 measured by phosphorylation of Smad2 (**Figure 7C-D**). These data indicate that $G_{\alpha q/11}$ is a
269 key component of CMS-induced TGF β signalling in both murine and human fibroblasts.

270 Previous studies have reported that $G_{\alpha q/11}$ -induces TGF β activation via the Rho-ROCK
271 cascade and αv integrins in epithelial cells (Xu et al. 2009; Froese et al. 2016). As $\alpha v\beta 1$,
272 $\alpha v\beta 3$, and $\alpha v\beta 5$ integrins are expressed by myofibroblasts and are involved in TGF β
273 activation (Pakshir et al. 2020), we utilised chemical inhibition of these integrins and ROCK
274 in our CMS model. When human fibroblasts were subject to breathing-related CMS in the
275 presence of a ROCK1/2 inhibitor (Y27632), a pan αv integrin inhibitor (CWHM-12) or a $\beta 1$
276 integrin-specific inhibitor (NOTT199SS), CMS-induced TGF β signalling was not reduced
277 (**Figure S3**). These data imply a novel pathway for CMS-induced TGF β signalling in
278 mesenchymal cells which requires $G_{\alpha q/11}$, but is independent of ROCK and integrin
279 signalling.

280 **$G_{\alpha q/11}$ induces TGF $\beta 2$ production, which is then available for CMS-induced serine** 281 **protease-mediated activation**

282 Proteases can activate latent TGF β independently of integrins, therefore we assessed the
283 effect of protease inhibitors in our CMS-induced TGF β signalling system. A pan serine
284 protease inhibitor 4-(2-aminoethyl)benzenesulfonyl fluoride (AEBSF), decreased CMS-
285 induced Smad2 phosphorylation in HLFs (**Figure 8A-B**), whereas the MMP inhibitor GM-
286 6001 had no effect on CMS-induced TGF β signalling even at high concentrations (**Figure**
287 **8C-D**). These findings indicate that serine proteases mediate CMS-induced TGF β signalling
288 in mesenchymal cells.

289 As TGF $\beta 2$ is the only TGF β isoform that is not activated by integrins (Jenkins 2008), we
290 hypothesised that breathing-related CMS would predominantly activate the TGF $\beta 2$ isoform
291 in mesenchymal cells. While CMS did not influence TGF $\beta 2$ protein expression in HLFs,
292 HLFs with siRNA-induced *GNAQ* and *GNA11* knockdown expressed less TGF $\beta 2$ than HLFs
293 with intact $G_{\alpha q/11}$ signalling (**Figure 8E-F**), suggesting that $G_{\alpha q/11}$ plays a role in TGF $\beta 2$
294 production. Conversely, TGF $\beta 1$ protein expression was not affected by *GNAQ* and *GNA11*
295 knockdown in HLFs (**Figure 8G**), suggesting an isoform-specific effect.

296 To evaluate the role of this CMS-induced TGF $\beta 2$ signalling pathway in alveologenesis, we
297 assessed TGF $\beta 2$ expression in the lungs of mice from our mouse models. *Pdgfrb-Cre*^{+/+}
298 ;*Gnaq*^{fl/fl}; *Gna11*^{-/-} lungs had a significantly lower TGF $\beta 2$ immunostaining score than *Gna11*^{-/-}
299 control lungs (median immunostaining score 0.8 in *Pdgfrb-Cre/ERT2*^{+/+}; *Gnaq*^{fl/fl}; *Gna11*^{-/-}

300 lungs, compared with 2.7 in *Gna11*^{-/-} controls, p<0.03, **Figure 8I**). Similarly, *Pdgfrb-*
301 *Cre/ERT2*^{+/+}; *Gnaq*^{fl/fl}; *Gna11*^{-/-} mouse lungs also had reduced TGFβ2 deposition compared
302 with *Gna11*^{-/-} controls after 3 weeks of tamoxifen (median immunostaining score 0.8 in
303 *Pdgfrb-Cre/ERT2*^{+/+}; *Gnaq*^{fl/fl}; *Gna11*^{-/-} lungs compared with 2.2 in *Gna11*^{-/-} controls, p<0.03,
304 **Figure 8J**). These data demonstrate that lungs lacking mesenchymal G_{αq/11} have less
305 TGFβ2 available for breathing-related CMS-induced activation, and this may be important in
306 alveologenesis and the maintenance of normal lung structure in vivo.

307 **G_{αq/11} influences expression of PDGF signalling components**

308 Platelet-derived growth factor (PDGF) signalling is known to be important in alveolar
309 development, and interacts with TGFβ signalling in normal development and disease
310 (Gouveia, Betsholtz, and Andrae 2017, 2018). We therefore investigated how G_{αq/11}
311 signalling influences the expression of PDGF signalling components in fibroblasts.
312 *Gnaq*^{-/-}; *Gna11*^{-/-} MEFs expressed significantly lower levels of *Pdgfb* and *Pdgfd* mRNA
313 compared with wild-type cells (p=0.03, **Figure 9B, 9D**). There was not a statistically
314 significant difference in the expression of *Pdgfa*, *Pdgfc*, *Pdgfra*, or *Pdgfrb* mRNA expression
315 between *Gnaq*^{-/-}; *Gna11*^{-/-} and wild-type MEFs (**Figure 9A,C,E,F**), although there was a trend
316 to reduced *Pdgfa* expression in *Gnaq*^{-/-}; *Gna11*^{-/-} MEFs (p=0.06, **Figure 9A**). These data
317 imply that mesenchymal G_{αq/11} deletion influences the expression of PDGF signalling
318 components, and thus may regulate PDGF signalling.

319 Discussion

320 In this study, we used mice with a targeted deletion of G_{αq/11} in mesenchymal cells to
321 demonstrate that mesenchymal G_{αq/11} is essential for the development and maintenance of
322 normal alveoli. Loss of G_{αq/11}-mediated signalling in mesenchymal cells caused failure of the
323 myofibroblast differentiation and ECM synthetic function required for alveolar development
324 and the maintenance of the adult lung, and reduced mesenchymal cell TGFβ2 production is
325 a key factor in these processes. In the absence of mesenchymal G_{αq/11}, TGFβ2 is
326 unavailable for activation by CMS-induced serine proteases thereby diminishing downstream
327 TGFβ signalling in both developing and adult lungs. These findings establish a previously
328 undescribed role for breathing-related CMS in TGFβ2 generation, and suggest a role for
329 TGFβ2 in alveolar development and lung homeostasis.

330 The role of G_{αq/11} in alveolar development has not previously been investigated, primarily
331 because germline G_{αq/11} deletion is embryonically lethal (Offermanns et al. 1998) and murine
332 alveolarisation occurs entirely postnatally (Beauchemin et al. 2016). Cell type-specific *Gnaq*
333 and *Gna11* deletion in neural, cardiovascular, and haematological tissues have various
334 manifestations ranging from no phenotype to profound cardiac abnormalities associated with

335 perinatal death (Wettschureck et al. 2006; Wettschureck et al. 2004; Hoyer et al. 2010;
336 Sassmann et al. 2010; Wettschureck et al. 2005; Wettschureck et al. 2007; Wettschureck et
337 al. 2001). However, alveolar abnormalities have not been described in germline or
338 conditional $G_{\alpha q/11}$ knockout mice, suggesting a unique role for mesenchymal $G_{\alpha q/11}$ in alveolar
339 development and maintenance.

340 We propose that the key mechanisms underlying the abnormal alveologenesis and
341 emphysema in mice with mesenchymal $G_{\alpha q/11}$ deletion present from conception or induced in
342 adulthood, respectively, are failure of myofibroblast differentiation and synthetic function.
343 Both $Pdgfrb-Cre^{+/-};Gnaq^{fl/fl};Gna11^{-/-}$ and $Pdgfrb-Cre/ERT2^{+/-};Gnaq^{fl/fl};Gna11^{-/-}$ mice had lower
344 lung elastin deposition that controls. $Pdgfrb-Cre^{+/-};Gnaq^{fl/fl};Gna11^{-/-}$ lungs also contained
345 fewer myofibroblasts and less collagen compared with controls, and mesenchymal cells
346 lacking $G_{\alpha q/11}$ express less *Col1a1*, *Col3a1*, and *Ein* mRNA than cells with intact $G_{\alpha q/11}$. As
347 myofibroblasts induce secondary septation by depositing ECM proteins at the tips of
348 developing secondary septae, and loss of elastin is a key feature of emphysema (Ito et al.
349 2019), these data suggest that mesenchymal $G_{\alpha q/11}$ -induced myofibroblast differentiation and
350 function are required for alveolar development and homeostasis.

351 Secondary crest myofibroblasts (SCMFs) are known to derive from PDGFR α -expressing
352 precursors (Boström et al. 1996; Lindahl et al. 1997; McGowan et al. 2008; R. Li et al. 2018),
353 however the role of PDGFR β ⁺ precursors in the development of SCMFs has not been
354 described. While this study cannot definitively conclude that PDGFR β ⁺ precursors, such as
355 pericytes, differentiate into SCMFs, it does show a role for PDGFR β ⁺ cells in alveolarisation.
356 Whether this occurs via direct differentiation of SCMFs from PDGFR β ⁺ precursors, or via
357 paracrine signalling from PDGFR β ⁺ cells should be the topic of further study.

358 $Pdgfrb-Cre^{+/-};Gnaq^{fl/fl};Gna11^{-/-}$ mouse lungs also contained abnormal peripheral pulmonary
359 vessels, with a hypertrophic vascular smooth muscle layer. This could be explained by
360 hypoxaemia-induced pulmonary arterial hypertension (PAH) secondary to the profound
361 pulmonary defects, in combination with disturbed GPCR signalling, resulting in vascular
362 remodelling (Patel et al. 2018; Cheng et al. 2012). However, $Pdgfrb-Cre^{+/-};Gnaq^{fl/fl};Gna11^{-/-}$
363 mice did not exhibit signs of respiratory distress at P14, and cardiac histology did not show
364 evidence of right ventricular hypertrophy, which would be expected in PAH. We hypothesise
365 that $G_{\alpha q/11}$ deletion prevents pericytes from migrating away from the perivascular region to
366 the alveolar parenchyma, resulting in dysregulated vascular smooth muscle growth.
367 However, firm conclusions on the cause of the abnormal peripheral pulmonary vessels in
368 $Pdgfrb-Cre^{+/-};Gnaq^{fl/fl};Gna11^{-/-}$ mice cannot be drawn from this work.

369 Altered CMS-induced TGF β activation is likely to be a key driver of the lung phenotypes
370 observed in *Pdgfrb-Cre^{+/-};Gnaq^{fl/fl};Gna11^{-/-}* and *Pdgfrb-Cre^{+/-};Gnaq^{fl/fl};Gna11^{-/-}* mice. TGF β
371 drives myofibroblast differentiation, cellular migration, and ECM protein production (Harrell et
372 al. 2018), and deficiencies and genetic polymorphisms in TGF β signalling pathway
373 components have been associated with emphysema (Bonniaud et al. 2004; M. Li et al. 2011;
374 Hersh et al. 2009; Celedón et al. 2004). Both lung stretch and tightly-controlled TGF β
375 signalling are important for normal lung development and regeneration (Belcastro et al.
376 2015; Nakanishi et al. 2007; Chen et al. 2005; Chen et al. 2008; Sterner-Kock et al. 2002;
377 Pieretti et al. 2014; Deng et al. 2019; Gauldie et al. 2003; Vicencio et al. 2004; Alejandro-
378 Alcázar et al. 2008; Bonniaud et al. 2004; Donahoe, Longoni, and High 2016), and CMS has
379 been demonstrated to induce TGF β signalling in a number of models and organ systems
380 (Froese et al. 2016; John et al. 2016; Fujita et al. 2010; Furumatsu et al. 2013; Maeda et al.
381 2011; Russo et al. 2018; Wang et al. 2013). Using the same *Gnaq^{fl/fl};Gna11^{-/-}* mice used in
382 our study, John et al described age-related emphysema related to reduced stretch-induced
383 TGF β signalling in mice lacking G $\alpha_{q/11}$ in type II alveolar epithelial cells (John et al. 2016).
384 Open access RNA-Seq data on the LungMAP and IPF Cell Atlas databases show that in
385 human and mouse lung, PDGFR β -positive cells include pericytes, fibroblasts and
386 myofibroblasts (www.ipfcellatlas.com ; www.lungmap.net). We therefore used human lung
387 fibroblasts and murine embryonic fibroblasts to assess the role of mesenchymal G $\alpha_{q/11}$ in
388 CMS-induced TGF β signalling, and to demonstrate the generalisability of our findings across
389 species.

390 CMS-induced TGF β signalling in mesenchymal cells was dependent on serine proteases
391 and independent of αv integrins, contrary to previous work in lung slices and epithelial cells
392 (Froese et al. 2016; Xu et al. 2009). This indicated that TGF β 2, an isoform that is activated
393 by proteases but not integrins (Jenkins 2008), may be the primary TGF β isoform activated
394 by mesenchymal cell stretch. G $\alpha_{q/11}$ -deficient fibroblasts expressed less TGF β 2, but had
395 unchanged levels of TGF β 1, compared with cells that express G $\alpha_{q/11}$, suggesting a TGF β
396 isoform-specific effect of G $\alpha_{q/11}$ deletion. These data suggest a novel pathway in which
397 mesenchymal G $\alpha_{q/11}$ drives TGF β 2 production, which is then available for protease-mediated
398 activation.

399 This is the first study to propose an isoform-specific role for TGF β 2 in mammalian alveolar
400 development and lung homeostasis. The three TGF β isoforms are highly expressed during
401 lung development with distinct spatial and temporal expression patterns (Schmid et al.
402 1991), however little is known about the specific regulation of TGF β 2 signalling. *Tgfb2^{-/-}* mice
403 die shortly after birth from developmental abnormalities distinct from those seen in *Tgfb1^{-/-}* or
404 *Tgfb3^{-/-}* mice (Sanford et al. 1997; Shull et al. 1992; Kaartinen et al. 1995). *Tgfb2^{-/-}* mice have

405 no gross lung morphological abnormalities in late intrauterine gestation, however collapsed
406 conducting airways are found postnatally (Sanford et al. 1997). While the *Pdgfrb-Cre^{+/-}*
407 *;Gnaq^{fl/fl};Gna11^{-/-}* mice generated in the present study did not share phenotypic features
408 with *Tgfb2^{-/-}* mice, it is possible that TGFβ2 production by non-mesenchymal cells is sufficient
409 for normal prenatal development. Additionally, as alveolarisation occurs entirely postnatally
410 in mice, the role of TGFβ2 in alveolar development that we describe could not be observed
411 in *Tgfb2^{-/-}* mice due to perinatal death. Our data demonstrate that loss of mesenchymal
412 $G_{\alpha q/11}$ causes a loss of the precise control of TGFβ signalling in the lungs, resulting in
413 abnormal alveologenesis and loss of lung homeostasis in developed lungs. Further work is
414 required to understand the precise roles of individual TGFβ isoforms in these processes.

415 The PDGF family is known to be important in lung development and regeneration, with PDGFA
416 being particularly important in alveolar development (Gouveia, Betsholtz, and Andrae 2018;
417 Gouveia et al. 2020; Gokey et al. 2021). We found a trend towards reduced *Pdgfa*
418 expression in MEFs with $G_{\alpha q/11}$ deletion, as well as *Pdgfb* and *Pdgfc*, suggesting that $G_{\alpha q/11}$
419 signalling may interact with PDGF-related pathways. Postnatal deletion of *Pdgfra*, which
420 encodes the major receptor for PDGFA, reduces lung *Tgfb2*, but not *Tgfb1*, transcripts (C. Li
421 et al. 2019), further supporting a role for PDGF signalling in $G_{\alpha q/11}$ - and TGFβ2-driven
422 alveolar development and regeneration. However, elastin deposition during alveologenesis
423 may not be dependent on PDGFA (Gouveia et al. 2020), therefore PDGF-independent
424 pathways are also likely to be involved in driving the abnormalities in *Pdgfrb-Cre^{+/-}*
425 *;Gnaq^{fl/fl};Gna11^{-/-}* and *Pdgfrb-Cre/ERT2^{+/-};Gnaq^{fl/fl};Gna11^{-/-}* mouse lungs. As pulmonary
426 mesenchymal cells are predominantly PDGF receptor-expressing, rather than PDGF ligand
427 producing (Gouveia, Betsholtz, and Andrae 2017), and $G_{\alpha q/11}$ deletion did not alter *Pdgfra* or
428 *Pdgfrb* expression, we hypothesise that mesenchymal $G_{\alpha q/11}$ deletion reduces lung TGFβ2
429 signalling, which subsequently alters PDGF ligand expression by other cell types. However,
430 it was beyond the scope of this work to dissect the interactions between $G_{\alpha q/11}$, TGFβ2, and
431 PDGF signalling.

432 As PDGFRβ is a mesenchymal cell marker found outside of the lung, the other organs of
433 *Pdgfrb-Cre^{+/-};Gnaq^{fl/fl};Gna11^{-/-}* and *Pdgfrb-Cre/ERT2^{+/-};Gnaq^{fl/fl};Gna11^{-/-}* mice were examined
434 histologically. *Pdgfrb-Cre^{+/-};Gnaq^{fl/fl};Gna11^{-/-}* kidneys demonstrated expansion and
435 prominence of medullary mesenchymal cells. However, the kidneys of *Pdgfrb-Cre/ERT2^{+/-}*
436 *;Gnaq^{fl/fl};Gna11^{-/-}* mice were normal, supporting the hypothesis that abnormalities observed
437 in *Pdgfrb-Cre^{+/-};Gnaq^{fl/fl};Gna11^{-/-}* kidneys were developmental in nature.

438 The limitations of this study predominantly relate to the poor condition of *Pdgfrb-Cre^{+/-}*
439 *;Gnaq^{fl/fl};Gna11^{-/-}* mice, which limited the analyses to a single time point and precluded the
440 study of CMS in vivo. Furthermore, the growth restriction of *Pdgfrb-Cre^{+/-};Gnaq^{fl/fl};Gna11^{-/-}*

441 mice could have indicated a nutritional deficiency that could have contributed to delayed
442 alveolar development. While these animals did have renal abnormalities which may have
443 contributed to the poor condition and failure to thrive of *Pdgfrb-Cre^{+/-};Gnaq^{fl/fl};Gna11^{-/-}* mice,
444 the bowel appeared normal and mice with mesenchymal $G_{\alpha q/11}$ deletion induced in adulthood
445 had normal kidneys. This suggests a true pulmonary phenotype in mesenchymal $G_{\alpha q/11}$
446 knockout mice. Additionally, our in vitro data provide compelling evidence for a role for
447 mesenchymal $G_{\alpha q/11}$ in a key lung developmental signalling pathway, suggesting that
448 mesenchymal $G_{\alpha q/11}$ deletion generates a true lung developmental phenotype.

449 Furthermore, while we propose that abnormalities in pericyte differentiation and migration
450 underlie the defective alveologenesis and emphysema in mesenchymal $G_{\alpha q/11}$ knockout
451 mice, *Pdgfrb* is expressed by other cell types, including myofibroblasts, fibroblasts, and
452 vascular smooth muscle cells (Henderson et al. 2013). While it is possible that disturbed
453 TGF β signalling in these cell types contributed to the lung phenotype in mesenchymal $G_{\alpha q/11}$
454 knockout mice, pericytes are major progenitors for all these cell types, and are therefore
455 likely to have played a primary role in the abnormalities observed.

456 Finally, this study has not investigated the role of lung inflammation in mesenchymal $G_{\alpha q/11}$
457 knockout mice. TGF β regulates inflammation, and John et al showed that emphysema in
458 mice with a type II epithelial $G_{\alpha q/11}$ deletion was associated with lung inflammation and M2
459 macrophage polarisation (John *et al.*, 2016). The mononuclear cellular aggregates in the
460 lungs of mice with mesenchymal $G_{\alpha q/11}$ deletion induced in adulthood could indicate
461 abnormal inflammation in these mice. However, these cellular aggregates were not observed
462 in mice with a germline mesenchymal $G_{\alpha q/11}$ knockout, and it was not possible to fully define
463 the role of inflammation and the immune response in the emphysema observed in *Pdgfrb-*
464 *Cre/ERT2^{+/-};Gnaq^{fl/fl};Gna11^{-/-}* mice in our study.

465 In conclusion, this is the first study to generate mesenchymal $G_{\alpha q/11}$ deleted mice, and has
466 demonstrated a novel signalling pathway for CMS-induced TGF β 2 signalling in murine
467 embryonic and mature human mesenchymal cells that is important for alveologenesis and
468 maintenance of the normal lung. These findings could have implications for the treatment of
469 several conditions associated with dysregulated developmental and repair pathways,
470 including fibrosis and emphysema.

471 **Materials and Methods**

472

473 **Resource Availability**

474 Lead Contact

475

476 Further information and requests for resources and reagents should be directed to and will
477 be fulfilled by the Lead Contact, Amanda Goodwin (Amanda.Goodwin@nottingham.ac.uk).

478

479 Materials Availability

480

481 This study did not generate new unique reagents.

482

483 Data and Code Availability

484

485 This study did not analyse or generate any new datasets or code

486

487 **Experimental Model and Subject Details**

488

489 Animal Studies

490

491 **Husbandry**

492 Mice were housed under specific pathogen-free conditions, with standard food and water
493 available *ad libitum*. All animal experiments were performed in accordance with the Animals
494 (Scientific Procedures) Act 1986, and approved by the Animal Welfare and Ethical Review
495 Board at the University of Nottingham.

496 **Breeding strategy**

497 For the germline mouse studies, mice with floxed alleles for *Gnaq* and germline deficiency in
498 *Gna11* ($Gnaq^{fl/fl};Gna11^{-/-}$) were crossed with mice that express Cre recombinase under the
499 control of the *Pdgfrb* gene ($Pdgfrb-Cre^{+/+}$). $Pdgfrb-Cre^{+/+};Gnaq^{+/fl};Gna11^{+/+}$ offspring from this
500 F1 generation were then bred with $Gnaq^{fl/fl};Gna11^{-/-}$ founders to produce an F2 generation,
501 including $Pdgfrb-Cre^{+/+};Gnaq^{fl/fl};Gna11^{-/-}$ mice. The genetic background for all mice was

502 predominantly C57BL6, with a minimum of a six backcross generations. The generation of
503 *Gnaq^{fl/fl};Gna11^{-/-}* and *Pdgfrb-Cre^{+/-}* mice has been described previously (Foo et al. 2006;
504 Offermanns et al. 1998; Wettschureck et al. 2001).

505 For the tamoxifen-inducible mouse gene knockout studies, the same breeding strategy was
506 used as for the germline studies but substituting *Pdgfrb-Cre/ERT2^{+/-}* mice (Laboratories) for
507 *Pdgfrb-Cre^{+/-}* animals.

508 **Genotyping**

509 Mice were genotyped using DNA isolated from ear notch biopsies by PCR analysis with
510 allele-specific primers. Primer sequences: *Cre* transgene 5'- GCG GTC TGG CAG TAA AAA
511 CTA TC – 3', 5' - GTG AAA CAG CAT TGC TGT CAC TT – 3' (product 100bp); internal
512 positive control 5' - CTA GGC CAC AGA ATT GAA AGA TCT – 3', 5' - GTA GGT GGA AAT
513 TCT AGC ATC ATC C – 3' (product 324bp); *Gna11* wild-type 5' – AGC ATG CTG TAA GAC
514 CGT AG - 3', 5' – GCC CCT TGT ACA GAT GGC AG – 3' (product 820bp); *Gna11* knockout
515 5' - CAG GGG TAG GTG ATG ATT GTG – 3', 5' – GAC TAG TGA GAC GTG CTA CTT CC
516 - 3' (product 450bp); *Gnaq* wild-type and floxed alleles 5' – GCA TGC GTG TCC TTT ATG
517 TGA G 3', 5' – AGC TTA GTC TGG TGA CAG AAG – 3' (products: 600bp (wild type), 700bp
518 (floxed). For *Cre-ERT2*, the following primers were used: 5'- GAA CTG TCA CCG GGA GGA
519 - 3', 5' - AGG CAA ATT TTG GTG TAC GG – 3' (400bp product).

520 PCR products were analysed by electrophoresis on ethidium bromide-stained agarose gels.

521 Mice were genotyped at 2 weeks old (P14). Genotype ratios of F2 mice from the
522 *Gnaq^{fl/fl};Gna11^{-/-}* and *Pdgfrb-Cre^{+/-}* crosses were compared with the expected Mendelian
523 frequency (12.5% per genotype). Similarly, Genotype ratios of F2 mice from the
524 *Gnaq^{fl/fl};Gna11^{-/-}* and *Pdgfrb-Cre/ERT2^{+/-}* crosses were assessed, with an expected
525 frequency of 5% for each Cre-expressing genotype.

526

527 Human Cells

528 For in vitro experiments using human lung fibroblasts, cells from 4-6 donors were used per
529 group. Cells were used at passage 5-6 for all in vitro experiments.

530 Human lung fibroblasts (HLFs) were isolated from donated post-mortem or surgical lung
531 biopsy samples, from male and female donors with and without pulmonary fibrosis. For non-
532 fibrotic fibroblasts, cells were isolated from regions of lung distant from the area of primary
533 diagnosis. Tissue was cut into 1mm x 1mm pieces and placed 10mm apart in a 10cm cell
534 culture dish. Tissue was cultured in DMEM supplemented with 10% foetal calf serum (FCS,

535 Fisher), L-glutamine (4mM, Sigma), penicillin (200 units/ml, Sigma), streptomycin (0.2mg/ml,
536 Sigma), and amphotericin B (2.5µg/ml). Fibroblast outgrowth could be seen after 6-8 days.
537 Tissue was removed from the cell culture dish if it became detached, or when cells had
538 reached 80% confluency and were ready for passage. Cells were maintained in a humidified
539 incubator at 37°C, 5% CO₂/ 95% air, in Dulbecco's Modified Eagle's Medium (DMEM,
540 Sigma), supplemented with 10% foetal calf serum (FCS, Fisher), L-glutamine (4mM, Sigma),
541 penicillin (100 units/ml, Sigma) and streptomycin (0.1mg/ml, Sigma).

542 Murine Cells

543 Wild-type, *Gna12*^{-/-}; *Gna13*^{-/-}, and *Gnaq*^{-/-}; *Gna11*^{-/-} murine embryonic fibroblasts (MEFs) were
544 a gift from Dr Stefan Offermanns, and their generation has been described elsewhere
545 (Zywietz et al. 2001; Gu et al. 2002). *Gnaq*, *Gna11*, *Gna12*, and *Gna13* gene expression
546 was also confirmed in house prior to these studies. Cells were maintained in a humidified
547 incubator at 37°C, 5% CO₂/ 95% air, in Dulbecco's Modified Eagle's Medium (DMEM,
548 Sigma), supplemented with 10% foetal calf serum (FCS, Fisher), L-glutamine (4mM, Sigma),
549 penicillin (100 units/ml, Sigma) and streptomycin (0.1mg/ml, Sigma).

550 **Method details**

551 Mouse studies

552 ***Pdgfrb-Cre*^{+/-}; *Gnaq*^{*fl/fl*}; *Gna11*^{-/-} Mouse Phenotyping**

553 Litters were observed for signs of ill health daily from birth. Mice were weighed at P14. Male
554 and female mice were included in all analyses. Mice had not undergone any previous
555 procedures. All mice that survived to P14 were phenotyped and had organs collected.
556 Mouse phenotyping analyses were performed by an observer blinded to genotype. Genotype
557 information was not available to the phenotyping observer until all phenotyping and health
558 status data had been recorded.

559 **Tamoxifen-inducible gene knockouts**

560 *Pdgfrb-Cre/ERT2*^{+/-}; *Gnaq*^{*fl/fl*}; *Gna11*^{-/-} offspring and their littermates were kept under standard
561 conditions until 7 weeks of age (P49), when tamoxifen-containing chow (400mg/kg tamoxifen
562 citrate) was introduced *ad libitum*. Health scoring and weights were measured daily for 3
563 weeks as tamoxifen was administered. Animals were humanely killed after 3 weeks of
564 tamoxifen administration (at 10 weeks old, P70).

565 ***Organ Collection***

566 Mice were humanely killed by intraperitoneal injection of pentobarbital, and organs collected
567 for histological analyses. The lungs were perfused by injecting 40units/ml heparin sodium in
568 PBS (Wockhardt) into the right ventricle, and inflated by cannulating the trachea and filling
569 the lungs with 10% formalin (VWR) under gravity. The trachea was ligated, and the heart
570 and lungs removed en bloc. Livers and kidneys were also collected. Organs were kept in
571 10% formalin (VWR) for 24 hours before paraffin embedding and sectioning.

572 Tissue histology staining

573 3µm (lung, kidney), and 5µm (heart, liver) formalin-fixed paraffin embedded tissue sections
574 were deparaffinised in xylene and rehydrated in graded alcohols. Haematoxylin and eosin,
575 Verhoeff van Gieson (elastin), and picosirius red staining were performed as per standard
576 protocols using buffers and stains prepared in house and mounted in DPX.

577 Staining solutions made in house

578 The following histology solutions were generated in house: Weigert's iodine (2g potassium
579 iodide, 1g iodine, 100ml distilled water); Verheoff's solution (20ml 5% alcoholic
580 haematoxylin, 8ml 10% ferric chloride, 8ml Weigert's iodine); Van Gieson's solution (5ml
581 aqueous acid fuschin, 100ml saturated aqueous picric acid); Picro-sirius red solution (0.5g
582 Direct Red 80 (Sigma), 500ml saturated aqueous picric acid); Weigert's haematoxylin (1:1
583 ratio of Weigert's solution A and Weigert's solution B); Weigert's solution A (1%
584 haematoxylin in 100% ethanol); Weigert's solution B (4ml 30% ferric chloride, 1ml 12N
585 hydrochloric acid, 95ml water); Acidified water (5ml glacial acetic acid, 1l distilled water);
586 Acid/alcohol solution (70% ethanol, 0.1% hydrochloric acid).

587 ***Haematoxylin and eosin (H&E) stain***

588 After being deparaffinised and rehydrated, tissue sections were submerged in Mayers
589 haematoxylin (Fisher) for 2 minutes, acid/alcohol solution for 1 minute, then 1% eosin
590 solution (VWR) for 3 minutes. Sections were rinsed with tap water between each step, then
591 dehydrated and mounted.

592 ***Elastin (Verhoeff Van Gieson) stain***

593 Lung sections were deparaffinised and hydrated to distilled water, then stained in Verhoeff's
594 solution for 1 hour until the tissue was completely black. Sections were differentiated in 2%
595 ferric chloride until elastin fibres were seen on a grey background, incubated in 5% sodium
596 thiosulphate for 1 minute, and then washed in running tap water for 5 minutes. Sections

597 were then counterstained in Van Gieson's solution for 5 minutes, dehydrated and mounted
598 as above.

599 ***Picrosirius red stain***

600 Lung, kidney, and heart sections were deparaffinised and hydrated. Nuclei were stained with
601 Weigert's haematoxylin for 8 minutes, and then washed in running tap water for 5 minutes.
602 Sections were incubated in picrosirius red for 1 hour, washed in two changed of acidified
603 water, then dehydrated and mounted.

604 Immunostaining

605 Tissue sections were deparaffinised in xylene and rehydrated in graded alcohols. Heat-
606 mediated antigen retrieval was performed by boiling sections in a microwave for 20 minutes
607 in 10mM citric acid buffer (pH 6.0). Endogenous peroxidase activity was blocked by
608 incubating sections in 3% hydrogen peroxide in methanol for 30 minutes. Nonspecific
609 binding was blocked with 5% goat serum (Sigma) in 0.1% BSA/PBS. Sections were
610 incubated with primary antibody in 5% goat serum overnight at 4°C in a humidified chamber,
611 followed by incubations for 60 minutes with secondary antibody and 30 minutes with avidin-
612 biotin complex (Vector). Sections were then stained with diaminobenzidine (Sigma),
613 counterstained with Mayers haematoxylin (Sigma), and mounted in DPX (Sigma). Slides
614 were washed in PBS (Sigma) between incubation steps.

615 The following antibodies were used for immunohistochemistry: Rabbit anti- α SMA (Abcam,
616 ab5694; 1:500), rabbit anti-CD31 (Abcam, ab182981; 1:2000), rabbit anti-ki67 (Abcam,
617 ab15580; 1 μ g/ml), rabbit anti-pro-surfactant protein C (Sigma, Ab3786; 1:2000), rabbit anti-
618 TGF β 2 (Proteintech, 19999-1-AP; 1:3000), rabbit anti-elastin (Atlas, HPA056941; 1:100),
619 and biotinylated goat anti-rabbit IgG (Vector, BA1000; 1:200).

620 Image Quantification

621 ***Image acquisition***

622 Images of H&E, elastin, and IHC were taken using a Nikon 90i microscope and NIS-
623 Elements software v3.2 (Nikon). Polarised light imaging of picrosirius red stained samples
624 was performed using a Zeiss Axioplan microscope (Zeiss) and MicroManager 1.4 software
625 (Vale Lab, UCSF).

626 ***Staining quantification***

627 For all analyses of histology images, *Pdgfrb-Cre^{+/-};Gnaq^{fl/fl};Gna11^{-/-}* or *Pdgfrb-Cre/ERT2^{+/-}*
628 *;Gnaq^{fl/fl};Gna11^{-/-}* mice were compared with *Pdgfrb-Cre^{-/-};Gnaq^{fl/fl};Gna11^{-/-}* littermate controls

629 (labelled as *Gna11*^{-/-} controls). For histological analyses, four animals per genotype were
630 assessed to allow differences in histological appearances to be detected. All image
631 quantification was performed by an observer blinded to genotype. This observer was not
632 unblinded to genotype until all image quantification data had been recorded.

633 For quantitative analyses of the lungs, 5-10 images were assessed per set of lungs, covering
634 all lobes and avoiding major airways and central blood vessels. All morphometric analyses
635 were performed using NIS Elements software v3.2 (Nikon), with the exception of peripheral
636 pulmonary vessel thickness measurements and kidney measurements, which were
637 performed using CaseViewer 2.3 software (3D Histech).

638 For quantification of immunohistochemistry and elastin staining, the “count” feature of
639 ImageJ (NIH) was used. Elastin fibres were identified as thin black fibres on VVG stain, and
640 secondary crests were elastin positive if they had black staining that was not clearly a cell
641 nucleus on Verhoeff van Geison staining. For immunohistochemistry staining, a cell was
642 counted if it stained brown. Only nuclear DAB staining was counted for Ki67 quantification.
643 For α SMA quantification, the number of α SMA-positive secondary crests per 40 x field was
644 counted. For Ki67 and pro-SPC staining, the total number of cells per 40x field was
645 quantified by counting nuclei, and the proportion of Ki67 or pro-SPC positive cells calculated
646 by dividing the number of stained cells per image by the total number of cells per image.

647 For quantification of TGF β 2 staining, the following scoring system was used and 7 fields
648 (20x magnification) per mouse were analysed:

- 649 - **Score 0:** No cells stained.
- 650 - **Score 0.5:** 1-25 cells stained at low intensity
- 651 - **Score 1.0:** 1-25 cells stained at high intensity
- 652 - **Score 1.5:** 26-50 cells stained at low intensity
- 653 - **Score 2.0:** 26-50 cells stained at high intensity
- 654 - **Score 2.5:** >50 cells stained at low intensity
- 655 - **Score 3.0:** >50 cells stained at high intensity

656 ***Morphometry***

657 Mean linear intercept (MLI) analysis of airspace size was performed as previously described
658 (John et al. 2016). Briefly, 10x magnification images were overlaid with a grid comprised of
659 100 μ m squares, and “intercepts” between gridlines and airspace walls counted. The MLI
660 was calculated by dividing the length of each gridline was divided by the intercept count. For
661 alveolar wall thickness measurements, 40x magnification images were overlaid with five
662 equally spaced horizontal lines and the alveolar wall thickness measured at points where

663 lung tissue crossed each line using the “measure” function of NIS Elements. Mean MLI and
664 alveolar wall thickness values were calculated for each mouse from all measurements
665 across all images and data presented as median \pm interquartile range. For secondary crest
666 counts, 10x magnification images were used and secondary crests counted for each image.
667 For peripheral vessel wall thickness, ten random peripheral pulmonary vessels were
668 identified using CD31 staining. Maximal and minimum vessel wall thickness in μm was
669 measured using the “measure” function of CaseViewer. For assessment of right ventricular
670 hypertrophy, the left and right cardiac ventricular wall thickness was measured using
671 CaseViewer, and the right: left ventricular wall thickness ratio calculated.

672 Breathing-related cyclical stretch experiments

673 Cells were seeded at 2×10^5 cells per well on collagen I-coated Bioflex® 6 well culture plates
674 (Dunn Labortechnik) in DMEM supplemented with 10% FCS, L-glutamine (4mM), penicillin
675 (100 units/ml) and streptomycin (0.1mg/ml) and allowed to adhere for 24 hours. The culture
676 medium was changed to 1% FCS in DMEM with 4mM L-glutamine for 24 hours before
677 stretching commenced. The Flexcell® FX-5000T system (Flexcell International Corporation)
678 was used to apply cyclical stretch to cells in vitro, according to the manufacturer’s
679 instructions. MEFs were stretched at a frequency of 1Hz, and HLFs at 0.3Hz to mimic
680 breathing in the relevant organism. 15% elongation and a sine waveform were used for all
681 cyclical stretch experiments. Cyclical stretch was applied for 48 hours, except for
682 experiments using siRNA-induced *GNAQ* and *GNA11* knockdown, where 24 hours of
683 cyclical stretch was used. Unstretched control cells were cultured in identical conditions
684 alongside the Flexcell® apparatus. Cells were lysed in protein lysis buffer (Cell Signalling)
685 supplemented with phosphatase (Phos-Stop, Sigma) and protease (Complete Mini, Sigma)
686 inhibitors, and 20 μM PMSF. All experimental replicates were performed independently.

687 ***Chemical Inhibitors used in Cyclical Stretch System***

688 When used, inhibitor compounds were applied in DMEM supplemented with 1% FCS and
689 4mM L-glutamine 30 minutes before stretching commenced. The activin receptor-like kinase
690 (ALK5)/ type I TGF β -receptor kinase inhibitor SB-525334 (Sigma) was used at a
691 concentration of 50 μM . A ROCK inhibitor (Y27632, Sigma), pan- αv integrin inhibitor
692 (CWHM-12), β1 integrin inhibitor (NOTT199SS) matrix metalloproteinase (MMP) inhibitor
693 GM6001 (Sigma), and serine protease inhibitor AEBSF (Sigma) were used at varying
694 concentrations. Where inhibitors were dissolved in DMSO, the negative control cells were
695 treated with a DMSO concentration equivalent to that used in the highest inhibitor
696 concentration.

697 ***GNAQ and GNA11 siRNA***

698 SiRNAs for human *GNAQ* (Dharmacon ON-TARGET-plus SMARTpool *GNAQ*) and *GNA11*
699 (Dharmacon ON-TARGET-plus SMARTpool *GNA11*) were used to induce *GNAQ* and
700 *GNA11* knockdown. A non-targeting siRNA pool was used as a control (Dharmacon ON-
701 TARGET-plus non-targeting pool).

702 Cells were seeded at 1.5×10^5 cells per well of a 6 well Flexcell® plate in antibiotic-free
703 DMEM supplemented with 10% FCS and 4mM L-glutamine. The following day, *GNAQ* and
704 *GNA11* siRNA was applied at a concentration of 15nM each with 4µl/ml DharmaFECT 1
705 transfection reagent (Dharmacon) as per the manufacturer's protocol. At 48 hours after
706 transfection, the media was changed to DMEM supplemented with 1% FCS and 4mM L-
707 glutamine. Cyclical stretch was applied for 24 hours from 72 hours post-transfection. LPA
708 stimulation was applied for 4 hours from 72 hours post-transfection. $G_{\alpha q/11}$ knockdown was
709 confirmed by western blot and qPCR

710 Western blotting

711 Protein concentrations were determined by BCA assay using a commercially available kit
712 (ThermoFisher), according to the manufacturer's instructions. Equal amounts of protein (15-
713 25µg) were loaded per lane of a 10% SDS-polyacrylamide gel and subject to
714 electrophoresis, and transferred onto a polyvinylidene fluoride membrane (BioRad).
715 Membranes were blocked for 1 hour in either 5% non-fat milk (pSmad2, Smad2/3, αSMA,
716 $G_{\alpha q}$, $G_{\alpha 11}$, GAPDH) or 3% BSA (TGFβ1, TGFβ2) in tris-buffered saline containing 0.1%
717 Tween, pH 7.4 (TBST). Membranes were incubated overnight at 4°C in blocking buffer with
718 the appropriate primary antibody. Membranes were washed in TBST, then incubated for 1-2
719 hours in the appropriate HRP-conjugated secondary antibody in blocking buffer. Western
720 blots were analysed using chemilluminescence and exposure to film (GE Healthcare).
721 Where membranes were probed for two different proteins of the same molecular weight, i.e.
722 pSmad2 and Smad2, the membrane was stripped after analysis of pSmad2 using Western
723 Restore Stripping Buffer (Thermo-Fisher) for 5 minutes and re-blocked with 5% non-fat milk
724 before application of the second primary antibody.

725 The following antibodies were used for western blots: Rabbit anti-phospho-Smad2 (pSmad2)
726 (Cell Signaling Technology, 3808; 1:1000), rabbit anti-Smad2/3 (Cell Signaling Technology,
727 3102; 1:1000), rabbit anti-αSMA (Abcam, ab5694; 0.5µg/ml), rabbit anti-GAPDH (Abcam,
728 ab181603; 1:10,000), rabbit anti-TGFβ1 (ab92486; 4µg/ml), mouse anti-TGFβ2 (Abcam,
729 ab36495; 1:1000), rabbit anti $G_{\alpha 11}$ (Abcam, ab153951; 1:1000), goat anti- $G_{\alpha q}$ (Abcam,
730 ab128060; 0.1µg/ml), HRP-conjugated goat-anti-rabbit (Agilent, P044801-2; 1:3000), HRP-

731 conjugated rabbit-anti-goat (Agilent, P016002-2; 1:3000), HRP-conjugated rabbit anti-mouse
732 (Agilent, P0260022-2, 1:3000).

733

734 ***Densitometry Analysis of Western Blots***

735

736 Densitometry was performed using ImageJ (NIH) on scanned western blot images. JPEG
737 images were converted into greyscale images, and the software used to calculate
738 densitometry values for each band relative to the other bands. These relative densitometry
739 values were used to calculate the expression of protein relative to loading control using the
740 equation: Protein relative to loading control = protein densitometry value/ loading control
741 protein densitometry value

742

743 Quantitative PCR

744 RNA was isolated from in vitro experiments using the Machery-Nagel Nucleospin RNA
745 isolation kit according to the manufacturer's instructions. Complementary DNA (cDNA) was
746 reverse transcribed from 200µg RNA using Superscript IV Reverse Transcriptase (Thermo
747 Fisher) according to the manufacturer's protocol. Quantitative PCR was performed on cDNA
748 using gene-specific primers (see below), and an MXPro3000 qPCR machine (Stratagene) at
749 an annealing temperature of 60°C for 40 cycles. KAPA SYBR FastTaq (Sigma) was used for
750 qPCR of all genes other than *Pdgfa*, *Pdgfb*, *Pdgfc*, *Pdgfd*, *Pdgfra*, and *Pdgfrb*, for which
751 PerfeCTa SYBR Green Fastmix (VWR) was used. Amplification of a single PCR product was
752 confirmed by melting curve analysis. The delta-delta Ct method was used to quantify gene
753 expression relative to the housekeeping genes *Hprt* (mouse samples) or *B2M* (human
754 samples).

755 Primer sequences for mouse genes were: *Hprt* forward 5' – TGA AAG ACT TGC TCG AGA
756 TGT CA - 3', *Hprt* reverse 5' CCA GCA GGT CAG CAA AGA ACT 3', *Acta2* forward 5' GGG
757 ATC CTG ACG CTG AAG TA 3', *Acta2* reverse 5' GAC AGC ACA GCC TGA ATA GC 3',
758 *Eln* forward 5' GAT GGT GCA CAC CTT TGT TG 3', *Eln* reverse 5' CAG TGT GAG CCA
759 TCT CA 3', *Col1a1* forward 5' AGC TTT GTG CAC CTC CGG CT 3', *Col1a1* reverse 5' ACA
760 CAG CCG TGC CAT TGT GG 3', *Col3a1* forward 5' TTT GCA GCC TGG GCT CAT TT 3',
761 *Col3a1* reverse 5' AGG TAC CGA TTT GAA CAG ACT, *Pdgfa* forward 5' GAG ATA CCC
762 CGG GAG TTG A 3', *Pdgfa* reverse 5' TCT TGC AAA CTG CAG GAA TG 3', *Pdgfb* forward
763 5' TGA AAT GCT GAG CGA CCA C 3', *Pdgfb* reverse 5' AGC TTT CCA ACT CGA CTC C
764 3', *Pdgfc* forward 5' AGG TTG TCT CCT GGT CAA GC 3', *Pdgfc* reverse 5' CCT GCG TTT

765 CCT CTA CAC AC 3', *Pdgfd* forward 5'CCA AGG AAC CTG CTT CTG AC 3', *Pdgfd* reverse
 766 5' CTT GGA GGG ATC TCC TTG TG 3', *Pdgfra* forward 5' CAA ACC CTG AGA CCA CAA
 767 TG 3', *Pdgfra* reverse 5' TCC CCC AAC AGT AAC CCA AG 3', *Pdgfrb* forward TGC CTC
 768 AGC CAA ATG TCA CC 3', *Pdgfrb* reverse 5' TGC TCA CCA CCT CGT ATT CC 3'.

769 Primer sequences for human genes were: *GNAQ* forward 5' –
 770 GGACAGGAGAGGGTGGCAAG – 3', *GNAQ* reverse 5' – TGGGATCTTGAGTGTGTCCA –
 771 3', *GNA11* forward 5' – CCACTGCTTTGAGAACGTGA – 3', *GNA11* reverse 5'
 772 GCAGGTCCTTCTTGTTGAGG – 3', *B2M* forward 5'AATCCAAATGCGGCATCT3', *B2M*
 773 reverse 5'GAGTATGCCTGCCGTGTG3'.

774 Statistical Analyses

775 Statistical analyses were performed using GraphPad Prism 8.2 software (GraphPad). For
 776 experiments with group sizes of 5 or less, a non-parametric test was used. For experiments
 777 with group sizes of 6 or over, data were assessed for normality and a parametric test used if
 778 data followed a normal distribution.

779 Key Resources

REAGENT or RESOURCE	SOURCE	IDENTIFIER
Antibodies		
Rabbit anti-phospho-Smad2 (pSmad2)	Cell Signaling Technology	Cat# 3808L
Rabbit anti-Smad2/3	Cell Signaling Technology	Cat# 3102
Rabbit anti- α -smooth muscle actin (α SMA)	Abcam	Cat# ab5694
Rabbit anti-GAPDH	Abcam	Cat# ab181603
Rabbit anti-TGF β 1	Abcam	Cat# ab92486
Rabbit anti-elastin	Atlas	Cat # HPA056941
Mouse anti-TGF β 2	Abcam	Cat# ab36495
Rabbit anti G α 11	Abcam	Cat# ab153951
Goat anti-G α q	Abcam	Cat# ab128060
HRP-conjugated goat-anti-rabbit	Agilent	Cat# P044801-2
HRP-conjugated rabbit-anti-goat	Agilent	Cat# P016002-2

HRP-conjugated rabbit anti-mouse	Agilent	Cat# P0260022-2
Rabbit anti-CD31	Abcam	Cat# ab182981
Rabbit anti-ki67	Abcam	Cat# ab15580
Rabbit anti-pro-surfactant protein C	Sigma	Cat# Ab3786
Rabbit anti-TGF β 2	Proteintech	Cat# 19999-1-AP
Biotinylated goat anti-rabbit IgG	Vector	Cat# BA1000
Chemicals, Peptides, and Recombinant Proteins		
Protein lysis buffer	Cell Signaling Technology	Cat# 9803
Phos-stop phosphatase inhibitors	Sigma	Cat# 04906837001
Complete mini protease inhibitors	Sigma	Cat# 04693124001
PMSF	Sigma	Cat# P7626
SB-525334 (ALK5 inhibitor)	Sigma	Cat# S8822
Y27632 (ROCK inhibitor)	Sigma	Cat# Y0503
CWHM-12 (α v integrin inhibitor)	A gift from Dr David Griggs, University of St Louis. Now commercially available from various suppliers	https://www.medchemexpress.com/CWHM-12.html https://medkoo.com/products/11038 https://www.caymanchem.com/product/19480/cwhm12
NOTT199SS	School of Chemistry at the University of Nottingham	n/a
GM6001 (MMP inhibitor)	Sigma	Cat# CC1010
DharmaFECT 1 transfection reagent	Dharmacon	Cat# T-2001-01

10% formalin	VWR	Cat# 11699404
Mayers haematoxylin	Sigma	Cat# S1275
Eosin	VWR	Cat# 101411-524
Hydrogen peroxide	VWR	Cat# 23619.264
SIGMAFAST(TM) 3,3'-Diaminobenzidine tablets	Sigma	Cat# D4418
AEBSF (serine protease inhibitor)	Sigma	Cat# SBR00015
Western Restore Stripping Buffer	Thermo-Fisher	Cat# 21059
Ferric chloride (Iron(III) chloride)	Sigma	Cat# 157740
Iodine	Sigma	Cat# 326143
Potassium iodide	Sigma	Cat# 03124
Picric acid (in aqueous solution)	VWR	Cat# 84512.260
Acid fuschin	Sigma	Cat# F8129
Direct red 80	Sigma	Cat# 365548
Sodium thiosulphate	Scientific Laboratory Supplies	Cat# 72049
Haematoxylin	Sigma	Cat# H3136
Experimental Models: Cell Lines		
Human lung fibroblasts – primary cultures	Isolated and cultured in house (see methods for details)	n/a
Murine embryonic fibroblasts – wild-type	(Gu et al. 2002; Zywiets et al. 2001)	n/a
Murine embryonic fibroblasts – $Gnaq^{-/-};Gna11^{-/-}$	(Gu et al. 2002; Zywiets et al. 2001)	n/a
Murine embryonic fibroblasts – $Gna12^{-/-};Gna13^{-/-}$	(Gu et al. 2002; Zywiets et al. 2001)	n/a
Experimental Models: Organisms/Strains		

Pdgfrb-Cre ^{+/-} mice	Generation described in (Foo et al. 2006)	n/a
Pdgfrb-Cre/ERT2 ^{+/+} mice	Jackson Laboratories	Cat # 029684
Gnaq ^{f/f} ;Gna11 ^{-/-} mice	Generation described in (Offermanns et al. 1998; Wettschreck et al. 2001). Sperm stored in lab of origin.	n/a
Oligonucleotides		
Genotyping primers: Cre recombinase 5'- GCG GTC TGG CAG TAA AAA CTA TC – 3'; 5' - GTG AAA CAG CAT TGC TGT CAC TT – 3'	Eurofins (custom order)	n/a
Genotyping primers: internal positive control 5' - CTA GGC CAC AGA ATT GAA AGA TCT – 3' 5' - GTA GGT GGA AAT TCT AGC ATC C – 3'	Eurofins (custom order)	n/a
Genotyping primers: Gna11 wild type 5' – AGC ATG CTG TAA GAC CGT AG - 3' 5' – GCC CCT TGT ACA GAT GGC AG – 3'	Eurofins (custom order)	n/a
Genotyping primers: Gna11 knockout 5' - CAG GGG TAG GTG ATG ATT GTG – 3' 5' – GAC TAG TGA GAC GTG CTA CTT CC - 3'	Eurofins (custom order)	n/a
Genotyping primers: Gnaq 5' – GCA TGC GTG TCC TTT ATG TGA G 3' 5' – AGC TTA GTC TGG TGA CAG AAG – 3'	Eurofins (custom order)	n/a

Genotyping primers: Cre/ERT2 5'- GAA CTG TCA CCG GGA - 3' 5' - AGG CAA ATT TTG GTG TAC GG – 3'	Eurofins (custom order)	n/a
Human GNAQ siRNA (ON-TARGET-plus SMARTpool)	Dharmacon	Cat# L-008562-00-0005
Human GNA11 siRNA (ON-TARGET-plus SMARTpool)	Dharmacon	Cat# L-010860-00-0005
Non-targeting siRNA pool (ON-TARGET-plus SMARTpool)	Dharmacon	Cat# D-001810-10-05
Mouse Hprt primer forward: 5' – TGA AAG ACT TGC TCG AGA TGT CA - 3'	Eurofins (custom order)	n/a
Mouse Hprt primer reverse: 5' – CCA GCA GGT CAG CAA AGA ACT 3'	Eurofins (custom order)	n/a
Mouse Acta2 primer forward: 5' - GGG ATC CTG ACG CTG AAG TA – 3'	Eurofins (custom order)	n/a
Mouse Acta2 primer reverse: 5' – GAC AGC ACA GCC TGA ATA GC – 3'	Eurofins (custom order)	n/a
Mouse Eln primer forward: 5' GAT GGT GCA CAC CTT TGT TG 3'	Eurofins (custom order)	n/a
Mouse Eln primer reverse: 5' CAG TGT GAG CCA TCT CA 3'	Eurofins (custom order)	n/a
Mouse Col1a1 primer forward: 5' AGC TTT GTG CAC CTC CGG CT 3'	Eurofins (custom order)	n/a
Mouse Col1a1 primer reverse: 5' ACA CAG CCG TGC CAT TGT GG 3'	Eurofins (custom order)	n/a
Mouse Col3a1 primer forward: 5' TTT GCA GCC TGG GCT CAT TT 3'	Eurofins (custom order)	n/a
Mouse Col3a1 primer reverse: 5' AGG TAC CGA TTT GAA CAG ACT 3'	Eurofins (custom order)	n/a
Mouse <i>Pdgfa</i> primer forward: 5' GAG ATA CCC CGG GAG TTG A 3'	Eurofins (custom order)	n/a

Mouse <i>Pdgfa</i> primer reverse: 5' TCT TGC AAA CTG CAG GAA TG 3'	Eurofins (custom order)	n/a
Mouse <i>Pdgfb</i> primer forward: 5' TGA AAT GCT GAG CGA CCA C 3'	Eurofins (custom order)	n/a
Mouse <i>Pdgfb</i> primer reverse: 5' AGC TTT CCA ACT CGA CTC C 3'	Eurofins (custom order)	n/a
Mouse <i>Pdgfc</i> primer forward: 5' AGG TTG TCT CCT GGT CAA GC 3'	Eurofins (custom order)	n/a
Mouse <i>Pdgfc</i> primer reverse: 5' CCT GCG TTT CCT CTA CAC AC 3'	Eurofins (custom order)	n/a
Mouse <i>Pdgfd</i> primer forward: 5' CCA AGG AAC CTG CTT CTG AC 3'	Eurofins (custom order)	n/a
Mouse <i>Pdgfd</i> primer reverse: 5' CTT GGA GGG ATC TCC TTG TG 3'	Eurofins (custom order)	n/a
Mouse <i>Pdgfra</i> primer forward: 5' CAA ACC CTG AGA CCA CAA TG 3'	Eurofins (custom order)	n/a
Mouse <i>Pdgfra</i> primer reverse: 5' TCC CCC AAC AGT AAC CCA AG 3'	Eurofins (custom order)	n/a
Mouse <i>Pdgfrb</i> primer forward: TGC CTC AGC CAA ATG TCA CC 3'	Eurofins (custom order)	n/a
Mouse <i>Pdgfrb</i> primer reverse: 5' TGC TCA CCA CCT CGT ATT CC 3'	Eurofins (custom order)	n/a
Human GNAQ primer forward: 5' – GGACAGGAGAGGGTGGCAAG – 3'	Eurofins (custom order)	n/a
Human GNAQ primer reverse: 5' – TGGGATCTTGAGTGTGTCCA – 3'	Eurofins (custom order)	n/a
Human GNA11 primer forward: 5' – CCACTGCTTTGAGAACGTGA – 3'	Eurofins (custom order)	n/a
Human GNA11 primer reverse: 5' GCAGGTCCTTCTTGTTGAGG – 3'	Eurofins (custom order)	n/a

Human B2M primer forward: 5'-AATCCAAATGCGGCATCT-3'	Eurofins (custom order)	n/a
Human B2M primer reverse: 5'-GAGTATGCCTGCCGTGTG-3'	Eurofins (custom order)	n/a
Software and Algorithms		
Image J	NIH	https://imagej.nih.gov/ij/
NIH Elements v3.2	Nikon	https://www.microscope.healthcare.nikon.com/products/software/nis-elements/viewer
MicroManager 1.4	Vale lab, UCSF	https://micro-manager.org/
CaseViewer 2.3	3D Histech	https://www.3dhistech.com/
Prism	Graphpad	https://www.graphpad.com/scientific-software/prism/
Other		
Goat serum	Sigma	Cat# G9023
Avidin-Biotin complex	Vector	Cat# SP2001
DPX mountant	Sigma	Cat# 06522
Phosphate buffered saline	Sigma	Cat# P4417
Nikon 90i microscope	Nikon	n/a
Axioplan microscope	Zeiss	n/a
Dulbecco's modified eagles medium	Sigma	D5671
Foetal Calf Serum	Harlan UK Ltd	S-0001AE
L-glutamine	Sigma	G7513
Penicillin/ streptomycin	Sigma	P4458

Amphotericin B	Sigma	Cat# A2942
Collagen I-coated Bioflex® 6 well culture plates	Dunn Labortechnik	Cat# 3001-C
Flexcell® cell stretching system	Flexcell International Corporation	Cat# FX-5000T
BCA Assay kit	ThermoFisher	Cat# PN23227
Nucleospin RNA isolation kit	Machery-Nagel	Cat# 740955.250
Superscript IV Reverse Transcriptase	ThermoFisher	Cat# 18090050
KAPA SYBR FastTaq	Sigma	Cat# KK4618
PerfeCTa® SYBR Green Fastmix	VWR	Cat# 733-1382
MXPro3000 qPCR machine	Stratagene	
Heparin sodium 5000 units/ml	Wockhardt	Cat# FP1083
Polyvinylidene fluoride membrane	BioRad	Cat# 1620177
Hyperfilm for western blots	GE Healthcare	Cat# 28-9068-35
ECL reagent	GE Healthcare	Cat# RPN2134
Clarity ECL	BioRad	Cat# 1705061
Tamoxifen-containing chow (400mg/kg tamoxifen citrate)	Envigo	Cat# TD.55125.1

780

781

782

783

784 **Acknowledgements**

785 We thank Dr Thomas McNally (University of Nottingham, UK) and Dr David Griggs (St Louis
786 University, Missouri, USA) for supplying the compounds NOTT199SS and CWHM-12,
787 respectively. NOTT199SS was identified as part of an MSci Chemistry undergraduate
788 integrin drug discovery collaboration between the School of Chemistry at the University of
789 Nottingham and GlaxoSmithKline (GSK), supervised by Dr Simon Macdonald (GSK) and Dr
790 Thomas McNally (University of Nottingham). We also thank Dr Tim Kendall (University of
791 Edinburgh), for his opinion on the liver histology.

792 **Declarations of Interests**

793 GJ reports grants or contracts from Astra Zeneca, Biogen, Galecto, GlaxoSmithKline, Nordic
794 Biosciences, RedX, Plaint, consulting fees from Bristol Myers Squibb, Chiesi, Daewoong,
795 Veracyre, Resolution Therapeutics and Pliant, honoraria from Boehringer Ingelheim, Chiesi,
796 Roch, PatientMPower, AstraZeneca, advisory roles with Boehringer Ingelheim, Galapagos,
797 and Vicore, non-financial support from NuMedii, and is a Trustee for Action for Pulmonary
798 Fibrosis.

799 ATG, AEJ, CJ, AH, ALT, KS, MP, NCH, SO – no competing interests

800 **Funding**

801 This work was funded by a Medical Research Council Clinical Research Training Fellowship
802 held by ATG (MR P001327/1). ATG was also funded by a National Institute for Health
803 Research Academic Clinical Fellowship (2982) for part of this project. ALT was funded by a
804 Medical Research Foundation fellowship (MRFAUK-2015-312) during this work. GJ is
805 funded by a National Institute for Health Research Professorship (NIHR-RP-2017-08-ST2-
806 014). NCH is supported by a Wellcome Trust Senior Research Fellowship in Clinical Science
807 (219542/Z/19/Z).

808

809 **Author contributions**

810 ATG and GJ conceived project. ATG performed experiments, conducted image analysis,
811 and wrote the original draft manuscript. AEJ supervised and gave methodological guidance
812 for mouse phenotyping experiments and microscopy. CJ performed some of the
813 immunohistochemistry included in this work. ATG, AEJ, AH, and ALT conducted animal
814 monitoring and tissue collection. ALT established original cultures of human lung fibroblasts

815 used in this study. KS and MP provided expert guidance on the performing and interpretation
816 of kidney histology. NCH and SO provided and guided the breeding of *Pdgfrb-Cre^{+/-}* and
817 *Gnaq^{fl/fl};Gna11^{-/-}* mice, respectively. GJ supervised the entire project. All authors reviewed
818 the original draft manuscript and contributed to editing and preparation of the final
819 manuscript.

820 **References**

821

822 Alejandre-Alcázar, M. A., M. Michiels-Corsten, A. G. Vicencio, I. Reiss, J. Ryu, R. R. de
823 Krijger, G. G. Haddad, D. Tibboel, W. Seeger, O. Eickelberg, and R. E. Morty. 2008.
824 "TGF-beta signaling is dynamically regulated during the alveolarization of rodent and
825 human lungs." *Dev Dyn* 237 (1): 259-69. <https://doi.org/10.1002/dvdy.21403>.

826 Barron, L., S. A. Gharib, and J. S. Duffield. 2016. "Lung Pericytes and Resident Fibroblasts:
827 Busy Multitaskers." *Am J Pathol* 186 (10): 2519-31.
828 <https://doi.org/10.1016/j.ajpath.2016.07.004>.

829 Bartram, U., and C. P. Speer. 2004. "The role of transforming growth factor beta in lung
830 development and disease." *Chest* 125 (2): 754-65.
831 <https://doi.org/10.1378/chest.125.2.754>.

832 Beauchemin, K. J., J. M. Wells, A. T. Kho, V. M. Philip, D. Kamir, I. S. Kohane, J. H. Graber,
833 and C. J. Bult. 2016. "Temporal dynamics of the developing lung transcriptome in
834 three common inbred strains of laboratory mice reveals multiple stages of postnatal
835 alveolar development." *PeerJ* 4: e2318. <https://doi.org/10.7717/peerj.2318>.

836 Belcastro, R., L. Lopez, J. Li, A. Masood, and A. K. Tanswell. 2015. "Chronic lung injury in
837 the neonatal rat: up-regulation of TGFβ1 and nitration of IGF-R1 by peroxynitrite as
838 likely contributors to impaired alveologenesis." *Free Radic Biol Med* 80: 1-11.
839 <https://doi.org/10.1016/j.freeradbiomed.2014.12.011>.

840 Bonniaud, P., M. Kolb, T. Galt, J. Robertson, C. Robbins, M. Stampfli, C. Lavery, P. J.
841 Margetts, A. B. Roberts, and J. Gauldie. 2004. "Smad3 null mice develop airspace
842 enlargement and are resistant to TGF-beta-mediated pulmonary fibrosis." *J Immunol*
843 173 (3): 2099-108. <https://doi.org/10.1006/jim.2004.1526> [pii].
844 <http://www.ncbi.nlm.nih.gov/pubmed/15265946>.

845 Boström, H., K. Willetts, M. Pekny, P. Levéen, P. Lindahl, H. Hedstrand, M. Pekna, M.
846 Hellström, S. Gebre-Medhin, M. Schalling, M. Nilsson, S. Kurland, J. Törnell, J. K.
847 Heath, and C. Betsholtz. 1996. "PDGF-A signaling is a critical event in lung alveolar
848 myofibroblast development and alveogenesis." *Cell* 85 (6): 863-73.
849 [https://doi.org/10.1016/s0092-8674\(00\)81270-2](https://doi.org/10.1016/s0092-8674(00)81270-2).

850 Celedón, J. C., C. Lange, B. A. Raby, A. A. Litonjua, L. J. Palmer, D. L. DeMeo, J. J. Reilly,
851 D. J. Kwiatkowski, H. A. Chapman, N. Laird, J. S. Sylvia, M. Hernandez, F. E.
852 Speizer, S. T. Weiss, and E. K. Silverman. 2004. "The transforming growth factor-

- 853 beta1 (TGFB1) gene is associated with chronic obstructive pulmonary disease
854 (COPD)." *Hum Mol Genet* 13 (15): 1649-56. <https://doi.org/10.1093/hmg/ddh171>.
- 855 Chanda, D., E. Otoupalova, S. R. Smith, T. Volckaert, S. P. De Langhe, and V. J.
856 Thannickal. 2019. "Developmental pathways in the pathogenesis of lung fibrosis."
857 *Mol Aspects Med* 65: 56-69. <https://doi.org/10.1016/j.mam.2018.08.004>.
- 858 Chen, H., J. Sun, S. Buckley, C. Chen, D. Warburton, X. F. Wang, and W. Shi. 2005.
859 "Abnormal mouse lung alveolarization caused by Smad3 deficiency is a
860 developmental antecedent of centrilobular emphysema." *Am J Physiol Lung Cell Mol*
861 *Physiol* 288 (4): L683-91. <https://doi.org/10.1152/ajplung.00298.2004>.
- 862 Chen, H., F. Zhuang, Y. H. Liu, B. Xu, P. Del Moral, W. Deng, Y. Chai, M. Kolb, J. Gauldie,
863 D. Warburton, H. L. Moses, and W. Shi. 2008. "TGF-beta receptor II in epithelia
864 versus mesenchyme plays distinct roles in the developing lung." *Eur Respir J* 32 (2):
865 285-95. <https://doi.org/10.1183/09031936.00165407>.
- 866 Cheng, H. Y., A. Dong, M. Panchatcharam, P. Mueller, F. Yang, Z. Li, G. Mills, J. Chun, A. J.
867 Morris, and S. S. Smyth. 2012. "Lysophosphatidic acid signaling protects pulmonary
868 vasculature from hypoxia-induced remodeling." *Arterioscler Thromb Vasc Biol* 32 (1):
869 24-32. <https://doi.org/10.1161/atvbaha.111.234708>.
- 870 Deng, S., H. Zhang, W. Han, C. Guo, and C. Deng. 2019. "Transforming Growth Factor-β-
871 Neutralizing Antibodies Improve Alveolarization in the Oxygen-Exposed Newborn
872 Mouse Lung." *J Interferon Cytokine Res* 39 (2): 106-116.
873 <https://doi.org/10.1089/jir.2018.0080>.
- 874 Donahoe, P. K., M. Longoni, and F. A. High. 2016. "Polygenic Causes of Congenital
875 Diaphragmatic Hernia Produce Common Lung Pathologies." *Am J Pathol* 186 (10):
876 2532-43. <https://doi.org/10.1016/j.ajpath.2016.07.006>.
- 877 Foo, S. S., C. J. Turner, S. Adams, A. Compagni, D. Aubyn, N. Kogata, P. Lindblom, M.
878 Shani, D. Zicha, and R. H. Adams. 2006. "Ephrin-B2 controls cell motility and
879 adhesion during blood-vessel-wall assembly." *Cell* 124 (1): 161-73.
880 <https://doi.org/10.1016/j.cell.2005.10.034>.
- 881 Froese, A. R., C. Shimbori, P. S. Bellaye, M. Inman, S. Obex, S. Fatima, G. Jenkins, J.
882 Gauldie, K. Ask, and M. Kolb. 2016. "Stretch-induced Activation of Transforming
883 Growth Factor-beta1 in Pulmonary Fibrosis." *Am J Respir Crit Care Med* 194 (1): 84-
884 96. <https://doi.org/10.1164/rccm.201508-1638OC>.
885 <https://www.ncbi.nlm.nih.gov/pubmed/26771871>.
- 886 Fujita, H., M. Hida, K. Kanemoto, K. Fukuda, M. Nagata, and M. Awazu. 2010. "Cyclic
887 stretch induces proliferation and TGF-beta1-mediated apoptosis via p38 and ERK in
888 ureteric bud cells." *Am J Physiol Renal Physiol* 299 (3): F648-55.
889 <https://doi.org/10.1152/ajprenal.00402.2009>.
- 890 Funke, M., L. Knudsen, D. Lagares, S. Ebener, C. K. Probst, B. A. Fontaine, A. Franklin, M.
891 Kellner, M. Kuhnel, S. Matthieu, R. Grothausmann, J. Chun, J. D. Roberts, Jr., M.
892 Ochs, and A. M. Tager. 2016. "Lysophosphatidic Acid Signaling through the

- 893 Lysophosphatidic Acid-1 Receptor Is Required for Alveolarization." *Am J Respir Cell*
894 *Mol Biol* 55 (1): 105-16. <https://doi.org/10.1165/rcmb.2015-0152OC>.
- 895 Furumatsu, T., E. Matsumoto, T. Kanazawa, M. Fujii, Z. Lu, R. Kajiki, and T. Ozaki. 2013.
896 "Tensile strain increases expression of CCN2 and COL2A1 by activating TGF-beta-
897 Smad2/3 pathway in chondrocytic cells." *J Biomech* 46 (9): 1508-15.
898 <https://doi.org/10.1016/j.jbiomech.2013.03.028>.
- 899 Gauldie, J., T. Galt, P. Bonniaud, C. Robbins, M. Kelly, and D. Warburton. 2003. "Transfer of
900 the active form of transforming growth factor-beta 1 gene to newborn rat lung induces
901 changes consistent with bronchopulmonary dysplasia." *Am J Pathol* 163 (6): 2575-
902 84. [https://doi.org/10.1016/s0002-9440\(10\)63612-7](https://doi.org/10.1016/s0002-9440(10)63612-7).
- 903 Gokey, J. J., J. Snowball, J. Green, M. Waltamath, J. J. Spinney, K. E. Black, L. P. Hariri, Y.
904 Xu, and A. K. Perl. 2021. "Pretreatment of aged mice with retinoic acid supports
905 alveolar regeneration via upregulation of reciprocal PDGFA signalling." *Thorax* 76
906 (5): 456-467. <https://doi.org/10.1136/thoraxjnl-2020-214986>.
- 907 Gouveia, L., C. Betsholtz, and J. Andrae. 2017. "Expression analysis of platelet-derived
908 growth factor receptor alpha and its ligands in the developing mouse lung." *Physiol*
909 *Rep* 5 (6). <https://doi.org/10.14814/phy2.13092>.
- 910 ---. 2018. "PDGF-A signaling is required for secondary alveolar septation and controls
911 epithelial proliferation in the developing lung." *Development* 145 (7).
912 <https://doi.org/10.1242/dev.161976>.
- 913 Gouveia, L., S. Kraut, S. Hadzic, E. Vazquez-Liébanas, B. Kojonazarov, C. Y. Wu, C. Veith,
914 L. He, G. Mermelekas, R. T. Schermuly, N. Weissmann, C. Betsholtz, and J. Andrae.
915 2020. "Lung developmental arrest caused by PDGF-A deletion: consequences for
916 the adult mouse lung." *Am J Physiol Lung Cell Mol Physiol* 318 (4): L831-L843.
917 <https://doi.org/10.1152/ajplung.00295.2019>.
- 918 Gu, J. L., S. Muller, V. Mancino, S. Offermanns, and M. I. Simon. 2002. "Interaction of G
919 alpha(12) with G alpha(13) and G alpha(q) signaling pathways." *Proc Natl Acad Sci*
920 *U S A* 99 (14): 9352-7. <https://doi.org/10.1073/pnas.102291599>
921 102291599 [pii]. <http://www.ncbi.nlm.nih.gov/pubmed/12077299>.
- 922 Harrell, C. R., B. Simovic Markovic, C. Fellabaum, A. Arsenijevic, V. Djonov, and V.
923 Volarevic. 2018. "Molecular mechanisms underlying therapeutic potential of
924 pericytes." *J Biomed Sci* 25 (1): 21. <https://doi.org/10.1186/s12929-018-0423-7>.
- 925 Henderson, N. C., T. D. Arnold, Y. Katamura, M. M. Giacomini, J. D. Rodriguez, J. H.
926 McCarty, A. Pellicoro, E. Raschperger, C. Betsholtz, P. G. Ruminiski, D. W. Griggs,
927 M. J. Prinsen, J. J. Maher, J. P. Iredale, A. Lacy-Hulbert, R. H. Adams, and D.
928 Sheppard. 2013. "Targeting of alphav integrin identifies a core molecular pathway
929 that regulates fibrosis in several organs." *Nat Med* 19 (12): 1617-24.
930 <https://doi.org/10.1038/nm.3282>.
- 931 Hersh, C. P., N. N. Hansel, K. C. Barnes, D. A. Lomas, S. G. Pillai, H. O. Coxson, R. A.
932 Mathias, N. M. Rafaels, R. A. Wise, J. E. Connett, B. J. Klanderman, F. L. Jacobson,

- 933 R. Gill, A. A. Litonjua, D. Sparrow, J. J. Reilly, and E. K. Silverman. 2009.
934 "Transforming growth factor-beta receptor-3 is associated with pulmonary
935 emphysema." *Am J Respir Cell Mol Biol* 41 (3): 324-31.
936 <https://doi.org/10.1165/rcmb.2008-0427OC>.
- 937 Hoyer, D. P., S. Gronke, K. F. Frank, K. Addicks, N. Wettschureck, S. Offermanns, E.
938 Erdmann, and H. Reuter. 2010. "Diabetes-related defects in sarcoplasmic Ca²⁺
939 release are prevented by inactivation of G(alpha)11 and G(alpha)q in murine
940 cardiomyocytes." *Mol Cell Biochem* 341 (1-2): 235-44.
941 <https://doi.org/10.1007/s11010-010-0454-1>.
- 942 Ito, J. T., J. D. Lourenço, R. F. Righetti, Iflc Tibério, C. M. Prado, and Fdtqs Lopes. 2019.
943 "Extracellular Matrix Component Remodeling in Respiratory Diseases: What Has
944 Been Found in Clinical and Experimental Studies?" *Cells* 8 (4).
945 <https://doi.org/10.3390/cells8040342>.
- 946 Jenkins, G. 2008. "The role of proteases in transforming growth factor-beta activation." *Int J*
947 *Biochem Cell Biol* 40 (6-7): 1068-78. [https://doi.org/S1357-2725\(07\)00403-7](https://doi.org/S1357-2725(07)00403-7) [pii]
948 10.1016/j.biocel.2007.11.026. <http://www.ncbi.nlm.nih.gov/pubmed/18243766>.
- 949 John, A. E., M. R. Wilson, A. Habgood, J. Porte, A. L. Tatler, A. Stavrou, G. Miele, L. Jolly,
950 A. J. Knox, M. Takata, S. Offermanns, and R. G. Jenkins. 2016. "Loss of epithelial
951 Gq and G11 signaling inhibits TGFbeta production but promotes IL-33-mediated
952 macrophage polarization and emphysema." *Sci Signal* 9 (451): ra104.
953 <https://doi.org/10.1126/scisignal.aad5568>.
954 <https://www.ncbi.nlm.nih.gov/pubmed/27811142>.
- 955 Kaartinen, V., J. W. Voncken, C. Shuler, D. Warburton, D. Bu, N. Heisterkamp, and J.
956 Groffen. 1995. "Abnormal lung development and cleft palate in mice lacking TGF-
957 beta 3 indicates defects of epithelial-mesenchymal interaction." *Nat Genet* 11 (4):
958 415-21. <https://doi.org/10.1038/ng1295-415>.
- 959 Kato, K., R. Dieguez-Hurtado, D. Y. Park, S. P. Hong, S. Kato-Azuma, S. Adams, M.
960 Stehling, B. Trappmann, J. L. Wrana, G. Y. Koh, and R. H. Adams. 2018. "Pulmonary
961 pericytes regulate lung morphogenesis." *Nat Commun* 9 (1): 2448.
962 <https://doi.org/10.1038/s41467-018-04913-2>.
- 963 Kiermayer, C., M. Conrad, M. Schneider, J. Schmidt, and M. Brielmeier. 2007. "Optimization
964 of spatiotemporal gene inactivation in mouse heart by oral application of tamoxifen
965 citrate." *Genesis* 45 (1): 11-6. <https://doi.org/10.1002/dvg.20244>.
- 966 Laboratory, Jackson. "029684 - B6.Cg-Tg(Pdgfrb-cre/ERT2)6096Rha/J (jax.org)." Accessed
967 21st January 2021.
- 968 Li, C., M. K. Lee, F. Gao, S. Webster, H. Di, J. Duan, C. Y. Yang, N. Bhopal, N. Peinado, G.
969 Pryhuber, S. M. Smith, Z. Borok, S. Bellusci, and P. Minoo. 2019. "Secondary crest
970 myofibroblast PDGFR α controls the elastogenesis pathway via a secondary tier of
971 signaling networks during alveologenesis." *Development* 146 (15).
972 <https://doi.org/10.1242/dev.176354>.

- 973 Li, C., M. Li, S. Li, Y. Xing, C. Y. Yang, A. Li, Z. Borok, S. De Langhe, and P. Minoo. 2015.
974 "Progenitors of secondary crest myofibroblasts are developmentally committed in
975 early lung mesoderm." *Stem Cells* 33 (3): 999-1012.
976 <https://doi.org/10.1002/stem.1911>.
- 977 Li, M., M. S. Krishnaveni, C. Li, B. Zhou, Y. Xing, A. Banfalvi, A. Li, V. Lombardi, O. Akbari,
978 Z. Borok, and P. Minoo. 2011. "Epithelium-specific deletion of TGF- β receptor type II
979 protects mice from bleomycin-induced pulmonary fibrosis." *J Clin Invest* 121 (1): 277-
980 87. <https://doi.org/10.1172/jci42090>.
- 981 Li, R., K. Bernau, N. Sandbo, J. Gu, S. Preissl, and X. Sun. 2018. "Pdgfra marks a cellular
982 lineage with distinct contributions to myofibroblasts in lung maturation and injury
983 response." *Elife* 7. <https://doi.org/10.7554/eLife.36865>.
- 984 Lindahl, P., L. Karlsson, M. Hellström, S. Gebre-Medhin, K. Willetts, J. K. Heath, and C.
985 Betsholtz. 1997. "Alveogenesis failure in PDGF-A-deficient mice is coupled to lack of
986 distal spreading of alveolar smooth muscle cell progenitors during lung
987 development." *Development* 124 (20): 3943-53.
988 <https://doi.org/10.1242/dev.124.20.3943>.
- 989 Lovering, A. T., J. E. Elliott, S. S. Laurie, K. M. Beasley, C. E. Gust, T. S. Mangum, I. M.
990 Gladstone, and J. W. Duke. 2014. "Ventilatory and sensory responses in adult
991 survivors of preterm birth and bronchopulmonary dysplasia with reduced exercise
992 capacity." *Ann Am Thorac Soc* 11 (10): 1528-37.
993 <https://doi.org/10.1513/AnnalsATS.201312-466OC>.
- 994 Maeda, T., T. Sakabe, A. Sunaga, K. Sakai, A. L. Rivera, D. R. Keene, T. Sasaki, E.
995 Stavnezer, J. Iannotti, R. Schweitzer, D. Ilic, H. Baskaran, and T. Sakai. 2011.
996 "Conversion of mechanical force into TGF-beta-mediated biochemical signals." *Curr*
997 *Biol* 21 (11): 933-41. <https://doi.org/10.1016/j.cub.2011.04.007>.
- 998 McGowan, S. E., R. E. Grossmann, P. W. Kimani, and A. J. Holmes. 2008. "Platelet-derived
999 growth factor receptor-alpha-expressing cells localize to the alveolar entry ring and
1000 have characteristics of myofibroblasts during pulmonary alveolar septal formation."
1001 *Anat Rec (Hoboken)* 291 (12): 1649-61. <https://doi.org/10.1002/ar.20764>.
- 1002 Mecham, R. P. 2018. "Elastin in lung development and disease pathogenesis." *Matrix Biol*
1003 73: 6-20. <https://doi.org/10.1016/j.matbio.2018.01.005>.
- 1004 Mizikova, I., and R. E. Morty. 2015. "The Extracellular Matrix in Bronchopulmonary
1005 Dysplasia: Target and Source." *Front Med (Lausanne)* 2: 91.
1006 <https://doi.org/10.3389/fmed.2015.00091>.
- 1007 Nakanishi, H., T. Sugiura, J. B. Streisand, S. M. Lonning, and J. D. Roberts, Jr. 2007. "TGF-
1008 beta-neutralizing antibodies improve pulmonary alveologenesi and vasculogenesis
1009 in the injured newborn lung." *Am J Physiol Lung Cell Mol Physiol* 293 (1): L151-61.
1010 <https://doi.org/10.1152/ajplung.00389.2006>.
- 1011 Offermanns, S., L. P. Zhao, A. Gohla, I. Sarosi, M. I. Simon, and T. M. Wilkie. 1998.
1012 "Embryonic cardiomyocyte hypoplasia and craniofacial defects in G alpha q/G alpha

- 1013 11-mutant mice." *EMBO J* 17 (15): 4304-12.
1014 <https://doi.org/10.1093/emboj/17.15.4304>.
1015 <http://www.ncbi.nlm.nih.gov/pubmed/9687499>.
- 1016 Pakshir, P., N. Noskovicova, M. Lodyga, D. O. Son, R. Schuster, A. Goodwin, H. Karvonen,
1017 and B. Hinz. 2020. "The myofibroblast at a glance." *J Cell Sci* 133 (13).
1018 <https://doi.org/10.1242/jcs.227900>.
- 1019 Patel, J. A., L. Shen, S. M. Hall, C. Benyahia, X. Norel, R. J. McNulty, S. Moledina, A. M.
1020 Silverstein, B. J. Whittle, and L. H. Clapp. 2018. "Prostanoid EP₂ Receptors Are Up-
1021 Regulated in Human Pulmonary Arterial Hypertension: A Key Anti-Proliferative
1022 Target for Treprostinil in Smooth Muscle Cells." *Int J Mol Sci* 19 (8).
1023 <https://doi.org/10.3390/ijms19082372>.
- 1024 Pieretti, A. C., A. M. Ahmed, J. D. Roberts, Jr., and C. M. Kelleher. 2014. "A novel in
1025 vitro model to study alveologenesis ." *Am J Respir Cell Mol Biol* 50 (2): 459-69.
1026 <https://doi.org/10.1165/rcmb.2013-0056OC>.
- 1027 Pozarska, A., J. A. Rodriguez-Castillo, D. E. Surate Solaligue, A. Ntokou, P. Rath, I.
1028 Mizikova, A. Madurga, K. Mayer, I. Vadasz, S. Herold, K. Ahlbrecht, W. Seeger, and
1029 R. E. Morty. 2017. "Stereological monitoring of mouse lung alveolarization from the
1030 early postnatal period to adulthood." *Am J Physiol Lung Cell Mol Physiol* 312 (6):
1031 L882-895. <https://doi.org/10.1152/ajplung.00492.2016>.
- 1032 Ricard, N., L. Tu, M. Le Hiress, A. Huertas, C. Phan, R. Thuillet, C. Sattler, E. Fadel, A.
1033 Seferian, D. Montani, P. Dorfmueller, M. Humbert, and C. Guignabert. 2014.
1034 "Increased pericyte coverage mediated by endothelial-derived fibroblast growth
1035 factor-2 and interleukin-6 is a source of smooth muscle-like cells in pulmonary
1036 hypertension." *Circulation* 129 (15): 1586-97.
1037 <https://doi.org/10.1161/circulationaha.113.007469>.
- 1038 Riccetti, M., J. J. Gokey, B. Aronow, and A. T. Perl. 2020. "The elephant in the lung:
1039 Integrating lineage-tracing, molecular markers, and single cell sequencing data to
1040 identify distinct fibroblast populations during lung development and regeneration."
1041 *Matrix Biol* 91-92: 51-74. <https://doi.org/10.1016/j.matbio.2020.05.002>.
- 1042 Russo, T. A., D. Stoll, H. B. Nader, and J. L. Dreyfuss. 2018. "Mechanical stretch
1043 implications for vascular endothelial cells: Altered extracellular matrix synthesis and
1044 remodeling in pathological conditions." *Life Sci* 213: 214-225.
1045 <https://doi.org/10.1016/j.lfs.2018.10.030>.
- 1046 Sanford, L. P., I. Ormsby, A. C. Gittenberger-de Groot, H. Sariola, R. Friedman, G. P. Boivin,
1047 E. L. Cardell, and T. Doetschman. 1997. "TGFbeta2 knockout mice have multiple
1048 developmental defects that are non-overlapping with other TGFbeta knockout
1049 phenotypes." *Development* 124 (13): 2659-70.
1050 <http://www.ncbi.nlm.nih.gov/pubmed/9217007>.
- 1051 Sassmann, A., B. Gier, H. J. Grone, G. Drews, S. Offermanns, and N. Wettschureck. 2010.
1052 "The Gq/G11-mediated signaling pathway is critical for autocrine potentiation of
1053 insulin secretion in mice." *J Clin Invest* 120 (6): 2184-93.
1054 <https://doi.org/10.1172/jci41541>.

- 1055 Schmid, P., D. Cox, G. Bilbe, R. Maier, and G. K. McMaster. 1991. "Differential expression
1056 of TGF beta 1, beta 2 and beta 3 genes during mouse embryogenesis." *Development*
1057 111 (1): 117-30.
- 1058 Shull, M. M., I. Ormsby, A. B. Kier, S. Pawlowski, R. J. Diebold, M. Yin, R. Allen, C. Sidman,
1059 G. Proetzel, D. Calvin, and et al. 1992. "Targeted disruption of the mouse
1060 transforming growth factor-beta 1 gene results in multifocal inflammatory disease."
1061 *Nature* 359 (6397): 693-9. <https://doi.org/10.1038/359693a0>.
1062 <http://www.ncbi.nlm.nih.gov/pubmed/1436033>.
- 1063 Sterner-Kock, A., I. S. Thorey, K. Koli, F. Wempe, J. Otte, T. Bangsow, K. Kuhlmeier, T.
1064 Kirchner, S. Jin, J. Keski-Oja, and H. von Melchner. 2002. "Disruption of the gene
1065 encoding the latent transforming growth factor-beta binding protein 4 (LTBP-4)
1066 causes abnormal lung development, cardiomyopathy, and colorectal cancer." *Genes*
1067 *Dev* 16 (17): 2264-73. <https://doi.org/10.1101/gad.229102>.
- 1068 Vicencio, A. G., C. G. Lee, S. J. Cho, O. Eickelberg, Y. Chuu, G. G. Haddad, and J. A. Elias.
1069 2004. "Conditional overexpression of bioactive transforming growth factor-beta1 in
1070 neonatal mouse lung: a new model for bronchopulmonary dysplasia?" *Am J Respir*
1071 *Cell Mol Biol* 31 (6): 650-6. <https://doi.org/10.1165/rcmb.2004-0092OC>.
- 1072 Wang, B. W., G. J. Wu, W. P. Cheng, and K. G. Shyu. 2013. "Mechanical stretch via
1073 transforming growth factor-beta1 activates microRNA-208a to regulate hypertrophy in
1074 cultured rat cardiac myocytes." *J Formos Med Assoc* 112 (10): 635-43.
1075 <https://doi.org/10.1016/j.jfma.2013.01.002>.
- 1076 Wettschureck, N., E. Lee, S. K. Libutti, S. Offermanns, P. G. Robey, and A. M. Spiegel.
1077 2007. "Parathyroid-specific double knockout of Gq and G11 alpha-subunits leads to a
1078 phenotype resembling germline knockout of the extracellular Ca²⁺-sensing
1079 receptor." *Mol Endocrinol* 21 (1): 274-80. <https://doi.org/10.1210/me.2006-0110>.
- 1080 Wettschureck, N., A. Moers, T. Hamalainen, T. Lemberger, G. Schutz, and S. Offermanns.
1081 2004. "Heterotrimeric G proteins of the Gq/11 family are crucial for the induction of
1082 maternal behavior in mice." *Mol Cell Biol* 24 (18): 8048-54.
1083 <https://doi.org/10.1128/mcb.24.18.8048-8054.2004>.
- 1084 Wettschureck, N., A. Moers, B. Wallenwein, A. F. Parlow, C. Maser-Gluth, and S.
1085 Offermanns. 2005. "Loss of Gq/11 family G proteins in the nervous system causes
1086 pituitary somatotroph hypoplasia and dwarfism in mice." *Mol Cell Biol* 25 (5): 1942-8.
1087 <https://doi.org/10.1128/mcb.25.5.1942-1948.2005>.
- 1088 Wettschureck, N., H. Rutten, A. Zywiets, D. Gehring, T. M. Wilkie, J. Chen, K. R. Chien, and
1089 S. Offermanns. 2001. "Absence of pressure overload induced myocardial
1090 hypertrophy after conditional inactivation of Galphaq/Galpha11 in cardiomyocytes."
1091 *Nat Med* 7 (11): 1236-40. <https://doi.org/10.1038/nm1101-1236>
1092 nm1101-1236 [pii]. <http://www.ncbi.nlm.nih.gov/pubmed/11689889>.
- 1093 Wettschureck, N., M. van der Stelt, H. Tsubokawa, H. Krestel, A. Moers, S. Petrosino, G.
1094 Schutz, V. Di Marzo, and S. Offermanns. 2006. "Forebrain-specific inactivation of
1095 Gq/G11 family G proteins results in age-dependent epilepsy and impaired

- 1096 endocannabinoid formation." *Mol Cell Biol* 26 (15): 5888-94.
1097 <https://doi.org/10.1128/mcb.00397-06>.
- 1098 www.ipfcellatlas.com. 2020. "IPF Cell Atlas Researchers. www.ipfcellatlas.com.
1099 Kaminski/Rosas dataset." Accessed 05/09/2020.
- 1100 www.lungmap.net. "LungMAP consortium. www.lungmap.net." Accessed 04/08/2020.
- 1101 Xu, M. Y., J. Porte, A. J. Knox, P. H. Weinreb, T. M. Maher, S. M. Violette, R. J. McAnulty, D.
1102 Sheppard, and G. Jenkins. 2009. "Lysophosphatidic acid induces alphavbeta6
1103 integrin-mediated TGF-beta activation via the LPA2 receptor and the small G protein
1104 G alpha(q)." *Am J Pathol* 174 (4): 1264-79.
1105 <https://doi.org/10.2353/ajpath.2009.080160>
- 1106 S0002-9440(10)60985-6 [pii]. <http://www.ncbi.nlm.nih.gov/pubmed/19147812>.
- 1107 Zywiets, A., A. Gohla, M. Schmelz, G. Schultz, and S. Offermanns. 2001. "Pleiotropic effects
1108 of Pasteurella multocida toxin are mediated by Gq-dependent and -independent
1109 mechanisms. involvement of Gq but not G11." *J Biol Chem* 276 (6): 3840-5.
1110 <https://doi.org/10.1074/jbc.M007819200>.
- 1111

1112 **Figure titles and legends**

1113

1114 Figure 1: *Pdgfrb-Cre^{+/+};Gnaq^{fl/fl};Gna11^{-/-}* mice are growth restricted

- 1115 A) Genotype frequencies from *Pdgfrb-Cre^{+/+} x Gnaq^{fl/fl};Gna11^{-/-}* breeding. Red line
1116 indicates the expected frequency for each genotype (n=30, 12.5%). Total n= 241, 24
1117 litters, mean litter size 7.4. Chi-squared value (χ^2) = 22.03, degrees of freedom =7,
1118 p<0.005.
- 1119 B) Body weights of P14 pups by genotype. Mean \pm SEM, one way ANOVA with Tukey's
1120 multiple comparisons test, n = 12 *Pdgfrb-Cre^{+/+} x Gnaq^{fl/fl};Gna11^{-/-}* mice, n= 21-43 for
1121 other genotypes.
- 1122 C) Photograph of a P14 pup with the *Pdgfrb-Cre^{+/+}; Gnaq^{fl/fl}; Gna11^{-/-}* genotype (left), and
1123 a *Gna11^{-/-}* littermate (right).
- 1124 D) Body weights of all pups from *Pdgfrb-Cre / Gnaq^{fl/fl}; Gna11^{-/-}* crosses by sex at P14.
1125 Mean \pm SEM, unpaired two-tailed Students T test, 88 female and 102 male mice.

1126 Figure 2: *Pdgfrb-Cre^{+/+};Gnaq^{fl/fl};Gna11^{-/-}* mice have abnormal lung appearances characteristic
1127 of disturbed alveologenesi

- 1128 A) Haematoxylin and eosin (H&E) (top), Ki67 immunohistochemistry (middle), and pro-
1129 SPC immunohistochemistry (bottom) staining of lungs from a P14 *Gna11^{-/-}* (left) and

- 1130 a *Pdgfrb-Cre^{+/-};Gnaq^{fl/fl};Gna11^{-/-}* mouse (right). Arrows on H&E images indicate
1131 secondary crests. Images representative of 4 mice per group. Scale bars show
1132 100µm.
- 1133 B) Mean linear intercept analysis of airspace size in P14 *Gna11^{-/-}* and *Pdgfrb-Cre^{+/-}*
1134 *;Gnaq^{fl/fl};Gna11^{-/-}* mice. Median ± interquartile range, n=4 mice per group, two-tailed
1135 Mann Whitney test.
- 1136 C) Alveolar wall thickness in P14 *Gna11^{-/-}* and *Pdgfrb-Cre^{+/-};Gnaq^{fl/fl};Gna11^{-/-}* mice.
1137 Median ± interquartile range, n=4 mice per group, two-tailed Mann Whitney test.
- 1138 D) Quantification of the number of secondary crests per 20 x field in P14 *Gna11^{-/-}* and
1139 *Pdgfrb-Cre^{+/-};Gnaq^{fl/fl};Gna11^{-/-}* mice. Median ± interquartile range, n=4 mice per
1140 group, two-tailed Mann Whitney test.
- 1141 E) Quantification of Ki67 immunohistochemistry in P14 *Gna11^{-/-}* and *Pdgfrb-Cre^{+/-}*
1142 *;Gnaq^{fl/fl};Gna11^{-/-}* mice. Shown as the percentage of Ki67 positive nuclei per 40x
1143 magnification field. Median ± interquartile range, n=4 mice per group, two-tailed
1144 Mann Whitney test.
- 1145 F) Quantification of Pro-SPC immunohistochemistry in P14 *Gna11^{-/-}* and *Pdgfrb-Cre^{+/-}*
1146 *;Gnaq^{fl/fl};Gna11^{-/-}* mice. Shown as the percentage of pro-SPC positive cells per 40x
1147 magnification field. Median ± interquartile range, n=4 mice per group, two-tailed
1148 Mann Whitney test.
- 1149 G) Relative lung to body weights in P14 *Gna11^{-/-}* and *Pdgfrb-Cre^{+/-};Gnaq^{fl/fl};Gna11^{-/-}*
1150 mice. Median ± interquartile range, n=5 *Pdgfrb-Cre^{+/-};Gnaq^{fl/fl};Gna11^{-/-}* mice, n=6
1151 *Gna11^{-/-}* controls, two-tailed Mann Whitney test.

1152 Figure 3: *Pdgfrb-Cre^{+/-};Gnaq^{fl/fl};Gna11^{-/-}* mice have reduced lung myofibroblast differentiation
1153 and function

- 1154 A) αSMA immunohistochemistry (row 1), elastin Verhoeff van Gieson stain (row 2),
1155 elastin immunohistochemistry (row 3), and picosirius red (PSR) staining (row 4-6)
1156 from P14 *Gna11^{-/-}* (left) and *Pdgfrb-Cre^{+/-};Gnaq^{fl/fl};Gna11^{-/-}* (right) mice. Arrows on
1157 elastin images shown elastin fibres. Picosirius red images shown are bright field
1158 (BF, row 4), polarised light (row 5), and bright field at high magnification (row 5).
1159 Representative images from 4 mice per genotype. Scale bars show 100µm (αSMA,
1160 PSR), 50µm (elastin VVG and IHC), and 10µm (picrosirius red high magnification).
- 1161 B) Quantification of the proportion of secondary crests that stained positively for αSMA
1162 in P14 *Gna11^{-/-}* and *Pdgfrb-Cre^{+/-};Gnaq^{fl/fl};Gna11^{-/-}* lungs. Median ± interquartile
1163 range, n=4 mice per group, two-tailed Mann Whitney test.
- 1164 C) *Acta2* mRNA expression in WT, *Gna12^{-/-};Gna13^{-/-}*, and *Gnaq^{-/-};Gna11^{-/-}* MEFs.
1165 Median ± interquartile range, n=4 per group, two-tailed Mann Whitney test.

- 1166 D) Representative western blot showing α SMA expression in wild-type (WT), *Gna12*^{-/-}
1167 ;*Gna13*^{-/-}, and *Gnaq*^{-/-};*Gna11*^{-/-} MEFs.
- 1168 E) Densitometry of western blots of α SMA expression in wild-type (WT), *Gna12*^{-/-}
1169 ;*Gna13*^{-/-}, and *Gnaq*^{-/-};*Gna11*^{-/-} MEFs. Median \pm interquartile range, n=4, two-tailed
1170 Mann Whitney test.
- 1171 F) The number of elastin fibres per high powered field (40 x magnification) in P14
1172 *Gna11*^{-/-} and *Pdgfrb-Cre*^{+/-};*Gnaq*^{fl/fl};*Gna11*^{-/-} lungs. Median \pm interquartile range, n=4
1173 mice per group, two-tailed Mann Whitney test.
- 1174 G) The proportion of secondary crests that stained positively for elastin in each high
1175 powered field (40 x magnification) in P14 *Gna11*^{-/-} and *Pdgfrb-Cre*^{+/-};*Gnaq*^{fl/fl};*Gna11*^{-/-}
1176 lungs. Median \pm interquartile range, n=4 mice per group, two-tailed Mann Whitney
1177 test.
- 1178 H) *Eln* mRNA expression in wild-type (WT) and *Gnaq*^{-/-};*Gna11*^{-/-} MEFs. Median \pm
1179 interquartile range, n=4, two-tailed Mann Whitney test.
- 1180 I) *Col1a1* mRNA expression in wild-type (WT) and *Gnaq*^{-/-};*Gna11*^{-/-} MEFs. Median \pm
1181 interquartile range, n=4, two-tailed Mann Whitney test.
- 1182 J) *Col3a1* mRNA expression in wild-type (WT) and *Gnaq*^{-/-};*Gna11*^{-/-} MEFs. Median \pm
1183 interquartile range, n=4, two-tailed Mann Whitney test.

1184 VVG = Verhoeff van Gieson; IHC = immunohistochemistry

1185 Figure 4: The lungs of *Pdgfrb-Cre*^{+/-};*Gnaq*^{fl/fl};*Gna11*^{-/-} mice contain abnormal peripheral
1186 pulmonary vessels.

1187 A-G) Lung sections from P14 *Pdgfrb-Cre*^{+/-};*Gnaq*^{fl/fl};*Gna11*^{-/-} mice were stained using various
1188 techniques.

- 1189 A) Haematoxylin and eosin stain. Scale bar shows 100 μ m.
- 1190 B) CD31 immunohistochemistry. Scale bar shows 10 μ m.
- 1191 C) α SMA immunohistochemistry. Scale bar shows 10 μ m.
- 1192 D) Ki67 immunohistochemistry. Scale bar shows 10 μ m.
- 1193 E) Picrosirius red stain (PSR). Same image shown using bright field (BF, E) and
1194 polarised light (PL, F) illumination). Scale bar shows 20 μ m.
- 1195 G) Elastin immunohistochemistry. Scale bar shows 50 μ m.
- 1196 H) Quantification of maximum peripheral vessel wall thickness in P14 *Gna11*^{-/-} and
1197 *Pdgfrb-Cre*^{+/-};*Gnaq*^{fl/fl};*Gna11*^{-/-} lungs. Median \pm interquartile range, n=4 mice per
1198 group, two-tailed Mann Whitney test.

- 1199 I) Quantification of minimum peripheral vessel wall thickness in P14 *Gna11*^{-/-} and
1200 *Pdgfrb-Cre*^{+/-};*Gnaq*^{fl/fl};*Gna11*^{-/-} lungs. Median ± interquartile range, n=4 mice per
1201 group, two-tailed Mann Whitney test.
- 1202 J) CD31 immunohistochemistry from P14 *Gna11*^{-/-} (left) and *Pdgfrb-Cre*^{+/-}
1203 ;*Gnaq*^{fl/fl};*Gna11*^{-/-} (right) mice. Representative images from 4 mice per genotype.
1204 Scale bars show 20µm.
- 1205 K) Haematoxylin and eosin stain of representative hearts from P14 *Gna11*^{-/-} (left) and
1206 *Pdgfrb-Cre*^{+/-};*Gnaq*^{fl/fl};*Gna11*^{-/-} (right) mice. Scale bars show 1000µm.
- 1207 L) Right: left cardiac ventricular wall thickness ratios in P14 *Gna11*^{-/-} (left) and *Pdgfrb-*
1208 *Cre*^{+/-};*Gnaq*^{fl/fl};*Gna11*^{-/-} (right) mice. Median ± interquartile range, n=3 mice per group,
1209

1210 Figure 5: *Pdgfrb-Cre*^{+/-};*Gnaq*^{fl/fl};*Gna11*^{-/-} have kidney abnormalities

- 1211 A) Haematoxylin and eosin, PDGFRβ immunohistochemistry, and αSMA
1212 immunohistochemistry of renal medulla, images of P14 *Gna11*^{-/-} and *Pdgfrb-Cre*^{+/-}
1213 ;*Gnaq*^{fl/fl};*Gna11*^{-/-} mouse kidneys. Representative images from 4 mice per genotype.
1214 Scale bars show 20µm.
- 1215 B) Low magnification images of haematoxylin and eosin staining of P14 *Gna11*^{-/-} (left)
1216 and *Pdgfrb-Cre*^{+/-};*Gnaq*^{fl/fl};*Gna11*^{-/-} (right) mice. Scale bars show 200µm.
- 1217 C) Cortex: medulla ratios of P14 *Gna11*^{-/-} and *Pdgfrb-Cre*^{+/-};*Gnaq*^{fl/fl};*Gna11*^{-/-} mice.
1218 Median ± interquartile range, n=4 mice per group, two-tailed Mann Whitney test.
- 1219 D) Relative kidney: total body weight in P14 *Gna11*^{-/-} and *Pdgfrb-Cre*^{+/-};*Gnaq*^{fl/fl};*Gna11*^{-/-}
1220 mice.

1221 Figure 6: Mice with mesenchymal *Gαq/11* deletion in adulthood develop emphysema

- 1222 A) Protocol for tamoxifen administration in *Pdgfrb-Cre/ERT2*^{+/-} x *Gnaq*^{fl/fl};*Gna11*^{-/-} mouse
1223 colony.
- 1224 B) Genotype frequencies from *Pdgfrb-Cre/ERT2*^{+/-} x *Gnaq*^{fl/fl};*Gna11*^{-/-} breeding. Red line
1225 indicates the expected frequency of *Pdgfrb-Cre/ERT2*^{+/-} genotypes (5%, n =5), and
1226 green line indicates expected frequency of *Pdgfrb-Cre/ERT2*^{-/-} genotypes (20%, n=
1227 22, total n=109, 20 litters, mean litter size 5.5.
- 1228 C) Weights of *Pdgfrb-Cre/ERT2*^{+/-};*Gnaq*^{fl/fl};*Gna11*^{-/-} mice (red) and littermates of all other
1229 genotypes (blue) during 21 days of tamoxifen administration.
- 1230 D) Histology of lungs from *Gna11*^{-/-} (left) and *Pdgfrb-Cre/ERT2*^{+/-};*Gnaq*^{fl/fl};*Gna11*^{-/-} (right)
1231 mice. Haematoxylin and eosin (row 1), elastin Verhoeff van Gieson (VVG, row 2),
1232 elastin immunohistochemistry (row 3), picrosirius red (PSR, row 4), and αSMA
1233 immunohistochemistry (row 5). Representative images from 4 mice per genotype.

1234 Scale bars show 50 μ m (H&E), 10 μ m (elastin VVG, PSR), 50 μ m (elastin IHC), and
1235 100 μ m (α SMA IHC).

1236 E) Mean linear intercept distance in *Gna11*^{-/-} and *Pdgfrb-Cre/ERT2*^{+/-};*Gnaq*^{fl/fl};*Gna11*^{-/-}
1237 mouse lungs. Median \pm interquartile range, n=4 mice per group, two-tailed Mann
1238 Whitney test.

1239 F) Quantification of elastin fibres in *Gna11*^{-/-} and *Pdgfrb-Cre/ERT2*^{+/-};*Gnaq*^{fl/fl};*Gna11*^{-/-}
1240 mouse lungs. Median \pm interquartile range, n=4 mice per group, two-tailed Mann
1241 Whitney test.

1242 G) Representative image of mononuclear cell infiltrates seen in *Pdgfrb-Cre/ERT2*^{+/-}
1243 ;*Gnaq*^{fl/fl};*Gna11*^{-/-} mouse lungs.

1244 Figure 7: $G_{\alpha q/11}$ mediates stretch-induced TGF β signalling in murine and human fibroblasts

1245 A) Representative western blot showing pSmad2 expression in wild-type (WT), *Gna12*^{-/-}
1246 ;*Gna13*^{-/-}, and *Gnaq*^{-/-}*Gna11*^{-/-} MEFs subject to cyclical stretch (15% elongation, 1Hz,
1247 48 hours).

1248 B) Densitometry of western blots from stretched MEFs shown as pSmad2 relative to
1249 Smad2 expression from 4 independent experiments. Median \pm interquartile range,
1250 n=4, two-tailed Mann Whitney Test.

1251 C) Representative western blot showing pSmad2 expression in HLFs treated with non-
1252 targeting (Scr) or *GNAQ* and *GNA11* siRNA then subject to cyclical stretch (15%
1253 elongation, 0.3Hz, 24 hours).

1254 D) Densitometry of western blots from stretched HLFs shown as pSmad2 relative to
1255 Smad2 expression from 4 independent experiments. Median \pm interquartile range,
1256 n=4, two-tailed Mann Whitney Test.

1257 + = stretched; - = unstretched

1258 Figure 8: $G_{\alpha q/11}$ signalling induces the production of TGF β 2 which is then available for
1259 stretch-induced serine protease-mediated activation

1260 A) Representative pSmad2 western blot of human lung fibroblasts treated with the
1261 serine protease inhibitor AEBSF then subject to cyclical stretch (15% elongation,
1262 0.3Hz, 48 hours).

1263 B) Relative pSmad2 to Smad2 densitometry of human lung fibroblasts treated with
1264 AEBSF then subject to cyclical stretch. Median \pm interquartile range, n=4, two-tailed
1265 Mann Whitney test.

1266 C) Representative pSmad2 western blot of human lung fibroblasts treated with the
1267 matrix metalloproteinase inhibitor GM6001 then subject to cyclical stretch (15%
1268 elongation, 0.3Hz, 48 hours).

- 1269 D) Relative pSmad2 to Smad2 densitometry from human lung fibroblasts treated with
1270 GM6001 then subject to cyclical stretch. Median \pm interquartile range, n=4, two-tailed
1271 Mann Whitney test.
- 1272 E) Representative TGF β 2 (top) and TGF β 1 (bottom) western blots of human lung
1273 fibroblasts subject to non-targeting (Scr) or *GNAQ* and *GNA11* siRNA and cyclical
1274 stretch (15% elongation, 0.3Hz, 24 hours).
- 1275 F) Relative TGF β 2 to GAPDH densitometry of human lung fibroblasts with and without
1276 siRNA-induced *GNAQ* and *GNA11* knockdown. Median \pm interquartile range, n=4,
1277 two-tailed Mann Whitney test
- 1278 G) Relative TGF β 1 to GAPDH densitometry of human lung fibroblasts with and without
1279 siRNA-induced *GNAQ* and *GNA11* knockdown. Median \pm interquartile range, n=4,
1280 two-tailed Mann Whitney test.
- 1281 H) TGF β 2 immunohistochemistry on P14 *Gna11*^{-/-} (left) and *Pdgfrb-Cre*^{+/-}
1282 ;*Gnaq*^{fl/fl};*Gna11*^{-/-} (right) mouse lungs (top row), and tamoxifen-treated P70 *Gna11*^{-/-}
1283 (left) and *Pdgfrb-Cre/ERT2*^{+/-};*Gnaq*^{fl/fl};*Gna11*^{-/-} mouse lungs.
- 1284 I) TGF β 2 immunohistochemistry scores of P14 *Gna11*^{-/-} (left) and *Pdgfrb-Cre*^{+/-}
1285 ;*Gnaq*^{fl/fl};*Gna11*^{-/-} (right) mouse lungs. Median \pm interquartile range, n=4, two-tailed
1286 Mann Whitney test.
- 1287 J) TGF β 2 immunohistochemistry scores of tamoxifen-treated P70 *Gna11*^{-/-} (left) and
1288 *Pdgfrb-Cre/ERT2*^{+/-};*Gnaq*^{fl/fl};*Gna11*^{-/-} (right) mouse lungs. Median \pm interquartile
1289 range, n=4, two-tailed Mann Whitney test.

1290 + = stretched; - = unstretched.

1291

1292 Figure 9: *G_{αq/11}* deletion influences expression of some PDGF transcripts in MEFs

1293 Relative mRNA expression of *Pdgfa* (A), *Pdgfb* (B), *Pdgfc* (C), *Pdgfd* (D), *Pgdfra* (E),
1294 and *Pdgfrb* (F) in wild-type (WT) and *Gnaq*^{-/-};*Gna11*^{+/-} MEFs. Median \pm interquartile
1295 range, n=4, two-tailed Mann Whitney test.

1296

1297

1298 **Supplemental Information titles and legends**

1299 Figure S1: *Pdgfrb-Cre^{+/-};Gnaq^{fl/fl};Gna11^{-/-}* mice have normal liver, heart, and bowel histology.

1300 Representative images of haematoxylin and eosin staining of liver (A), heart (B), and
1301 bowel (C) from *Gna11^{-/-}* and *Pdgfrb-Cre^{+/-};Gnaq^{fl/fl};Gna11^{-/-}* mice.

1302

1303 Figure S2: *Pdgfrb-Cre/ERT2^{+/-};Gnaq^{fl/fl};Gna11^{-/-}* mice have normal kidney histology after
1304 three weeks of tamoxifen.

1305 Representative images of haematoxylin and eosin staining of kidney (A) from *Gna11^{-/-}*
1306 and *Pdgfrb-Cre/ERT2^{+/-};Gnaq^{fl/fl};Gna11^{-/-}* mice treated with three weeks of
1307 tamoxifen.

1308

1309 Figure S3: Cyclical stretch-induced TGF β activation occurs independently of ROCK, and α
1310 and β 1 integrins in fibroblasts.

- 1311 A) Representative pSmad2 western blot of human lung fibroblasts treated with Y27632
1312 then subject to 48 hours of cyclical stretch (15% elongation, 0.3Hz, 48 hours).
1313 B) Relative pSmad2 to Smad2 densitometry from western blots of human lung
1314 fibroblasts treated with Y27632 then subject to cyclical stretch. Median \pm interquartile
1315 range, n=4, two-tailed Mann Whitney test.
1316 C) Representative pSmad2 western blot of human lung fibroblasts treated with an α
1317 integrin inhibitor (CWHM-12) then subject to 48 hours of cyclical stretch (15%
1318 elongation, 0.3Hz, 48 hours).
1319 D) Relative pSmad2 to Smad2 densitometry of human lung fibroblasts treated with
1320 CWHM-12 then subject to cyclical stretch. Median \pm interquartile range, n=4, two-
1321 tailed Mann Whitney test.
1322 E) Representative pSmad2 western blot of human lung fibroblasts treated with a β 1
1323 integrin inhibitor (NOTT199SS) then subject to 48 hours of cyclical stretch (15%
1324 elongation, 0.3Hz, 48 hours).
1325 F) pSmad2 relative to Smad2 densitometry of human lung fibroblasts treated with
1326 NOTT199SS then subject to cyclical stretch. Median \pm interquartile range, n=4, two-
1327 tailed Mann Whitney Test.

1328 + = stretched; - = unstretched. Alk5 inh = 50 μ M Alk5 inhibitor (SB525334)

1329

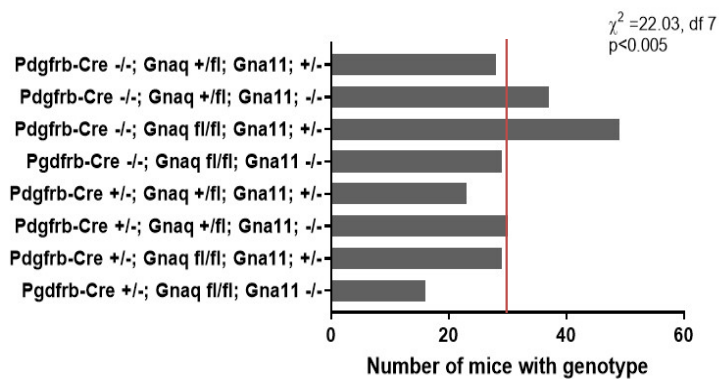
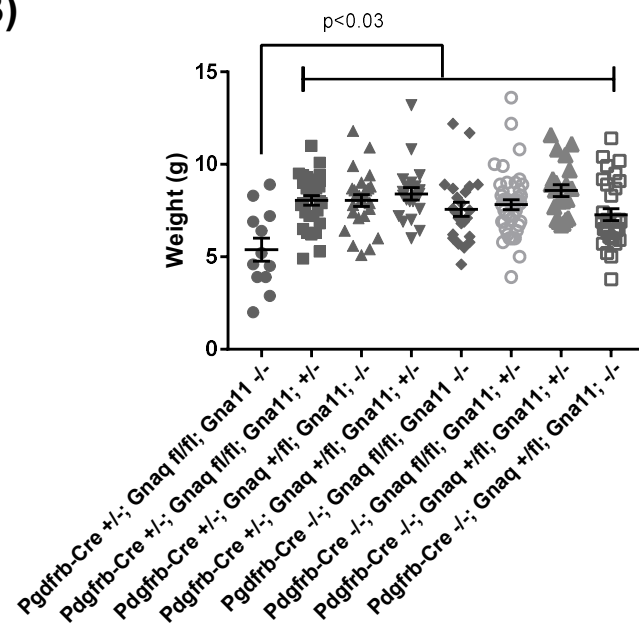
1330

1331

1332

Fig 1

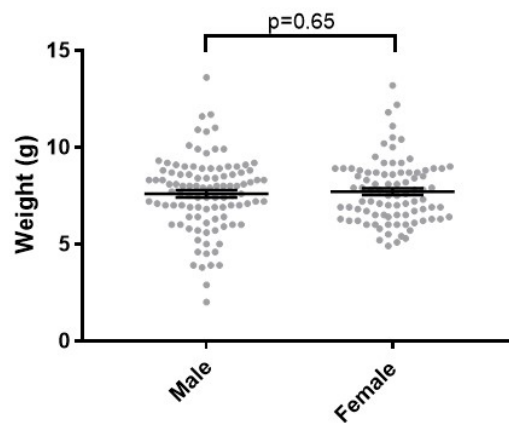
bioRxiv preprint doi: <https://doi.org/10.1101/2020.09.06.284778>; this version posted July 15, 2022. The copyright holder for this preprint (which was not certified by peer review) is the author/funder, who has granted bioRxiv a license to display the preprint in perpetuity. It is made available under aCC-BY-NC-ND 4.0 International license.

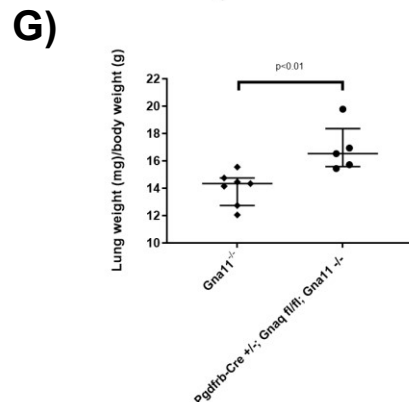
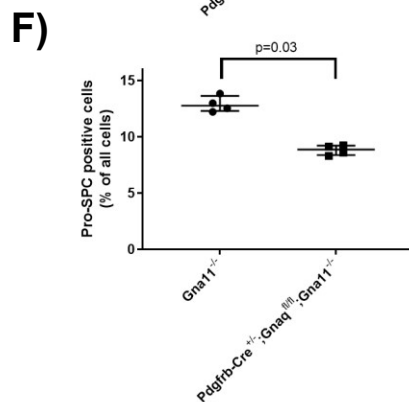
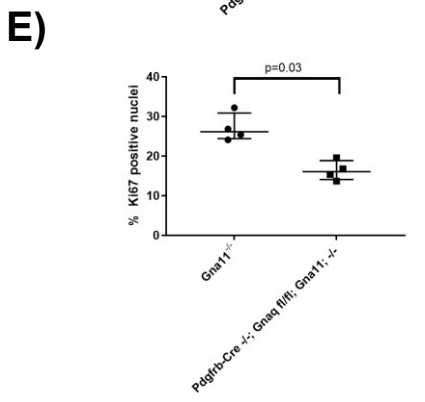
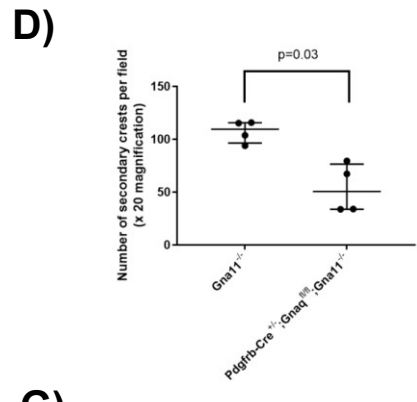
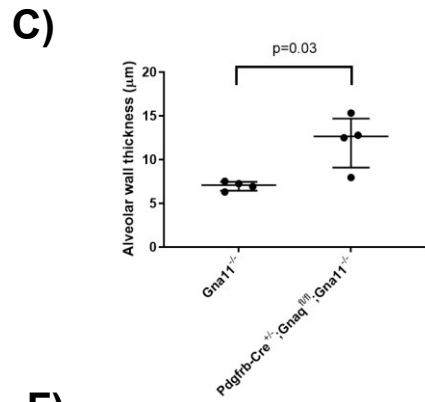
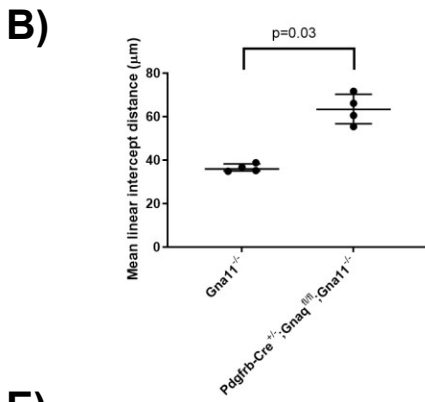
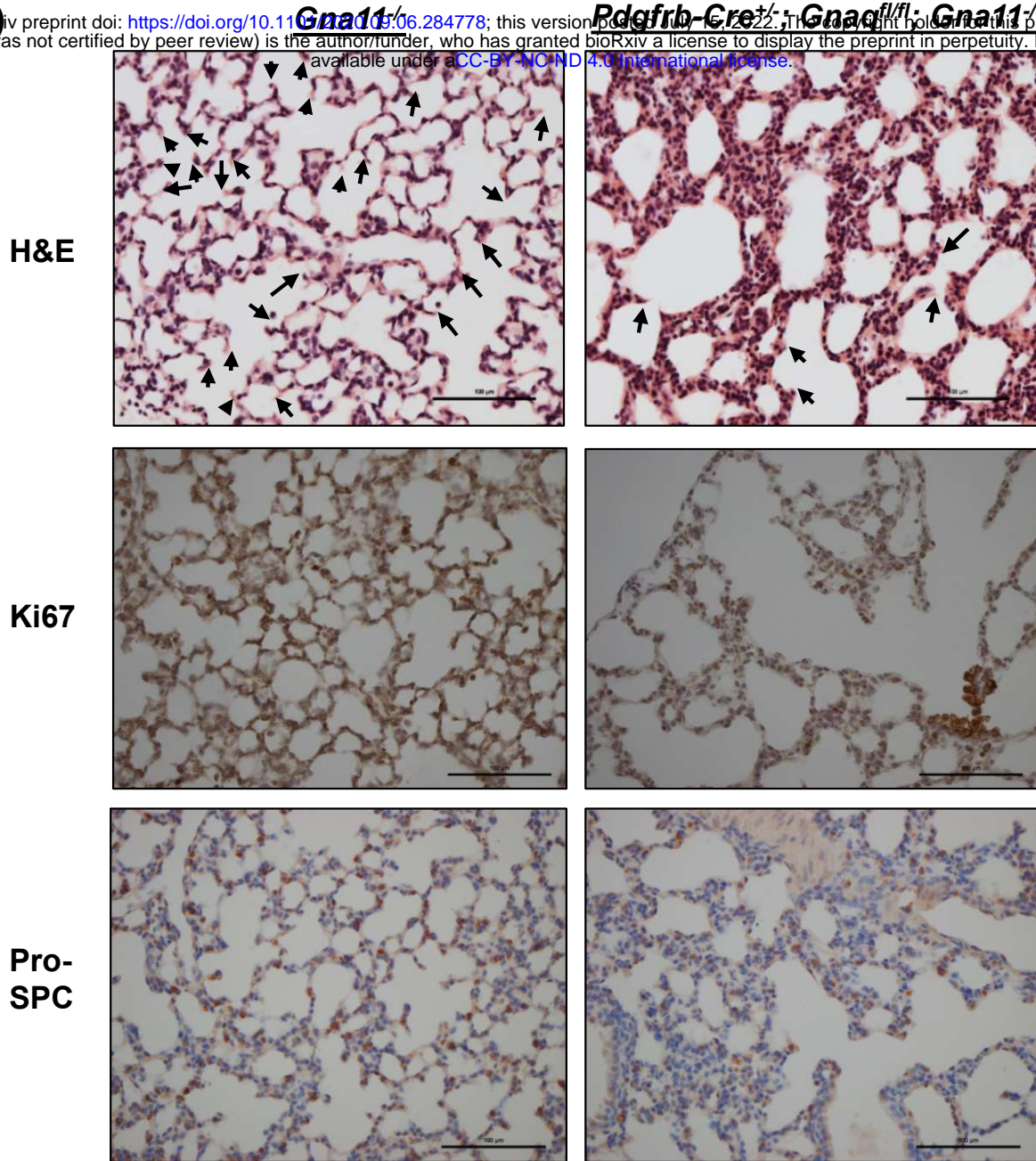
A)**B)****C)**

Pdgfrb-Cre^{+/-};
Gnaq^{fl/fl}; *Gna11*^{-/-}



Pdgfrb-Cre^{-/-};
Gnaq^{fl/fl}; *Gna11*^{-/-}

**D)**



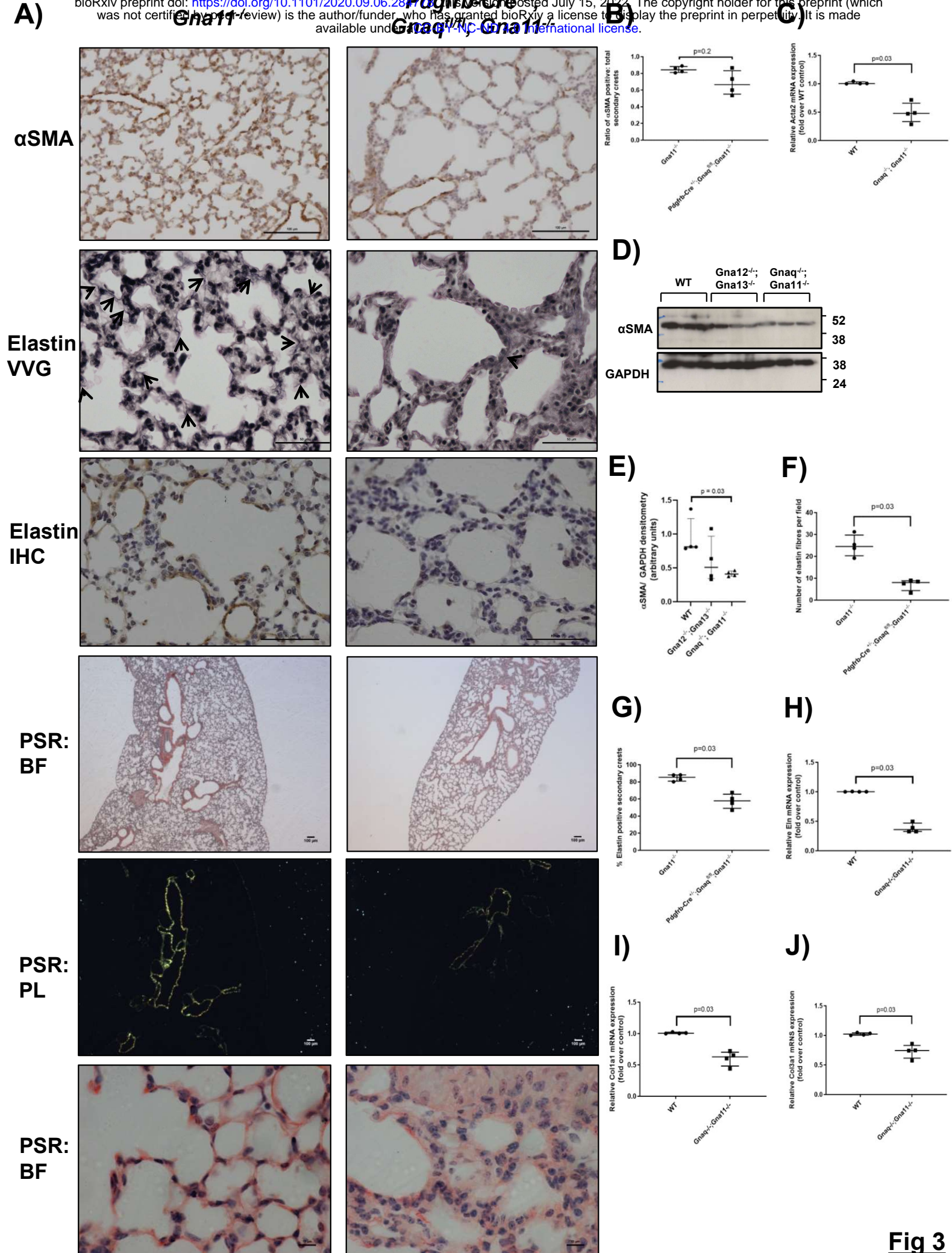


Fig 4

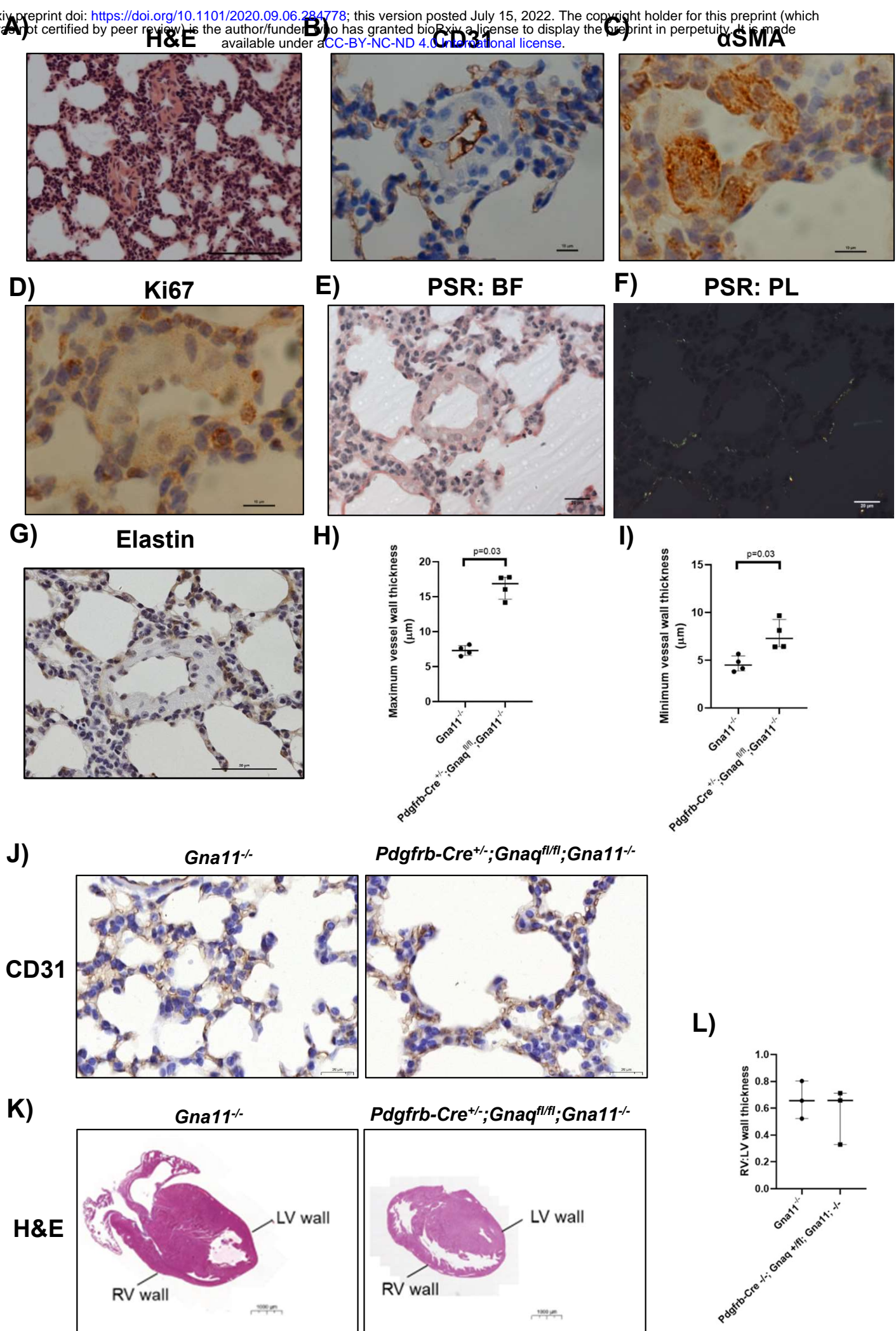
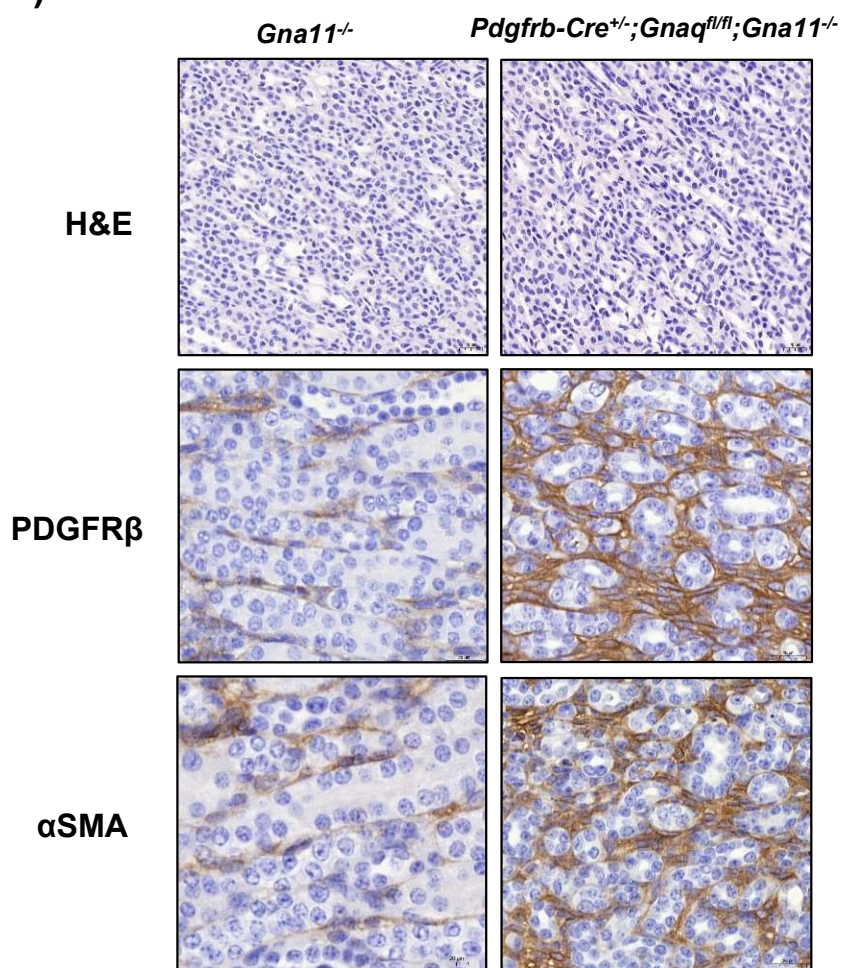
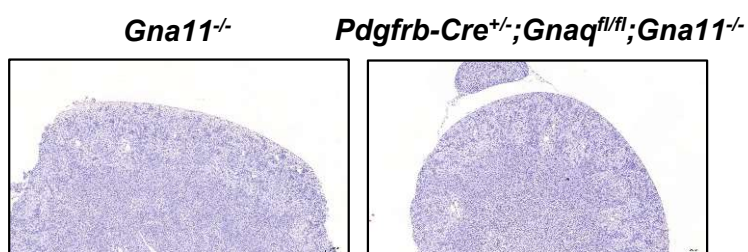


Fig 5

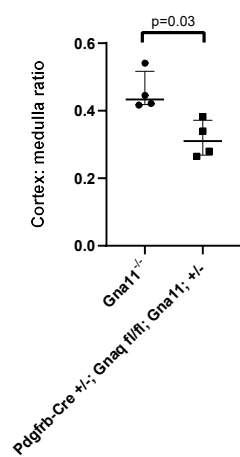
A)



B)



C)



D)

